An Overview of the Thermomechanical Processing of α/β Titanium Alloys: Current Status and Future Research Opportunities

S.L. SEMIATIN

Current understanding of the principles underlying the thermomechanical processing (TMP) of α/β titanium alloys is reviewed. Attention is focused on the formulation of constitutive descriptions for plastic flow under hot-working conditions, the evolution of microstructure, the occurrence of defects, and novel/emerging TMP techniques. With regard to constitutive behavior, descriptions of the plastic flow of the individual phases and two-phase alloys *per se* are summarized. The important influence of phase morphology, size, and volume fraction on plastic flow is emphasized. Mechanisms which underlie microstructure evolution include beta recrystallization (in the high-temperature β field), the development of dislocation substructure and its effect on dynamic and static spheroidization of colony microstructures (in the two-phase field), static and dynamic coarsening of primary α, and the development of deformation and transformation textures. In the area of defects, the effect of TMP variables and starting microstructure on the formation of cavities, the persistence of microtexture, and the development of undesirably-coarse β grain structures are described. The current status of relatively new processing techniques for α/β titanium alloys such as low-temperature superplastic forming and solid-state joining (*via* linear friction or friction-stir methods) are also briefly reviewed. Last, R&D which could help to resolve deficiencies in the current knowledge base for TMP of α/β titanium alloys are summarized for each of the areas.

I. INTRODUCTION

TITANIUM and its alloys find widespread use in the aerospace, marine, chemical, and other industries because of an attractive combination of mechanical properties, corrosion resistance, and light weight. Components of these materials can be produced by a variety of techniques including wrought, solidification/casting, and powder-metallurgy approaches.[1,2] From a tonnage standpoint, wrought methods based on the casting of ingots followed by various hot deformation and heat treatment operations, collectively referred to as thermomechanical processing (TMP), are the most common. In addition to producing a desired final shape in the form of a semi-finished mill product or a wrought part, the work introduced by deformation serves to accelerate desirable changes in microstructure both during hot working itself (*i.e.*, "dynamically") or "statically" during subsequent heat treatment.

Microstructure control during TMP typically relies upon the allotropic transformation of titanium from a high-temperature bcc (β) phase to a lower temperature hcp (α) phase and specific alloy composition chosen to stabilize a lesser or greater fraction of β at room temperature. Commercial alloys which are rich in α-stabilizing elements (*e.g.*, Al, O) and lean in β stabilizing elements (*e.g.*, V, Mo, Fe) consist of the so-called single-phase α, near-α, and α/β titanium classes. By contrast, Ti alloys with large amounts of β-stabilizing elements are typically grouped into near-β, metastable β, and β alloy classes.[1,2] The alloy class and the temperature above which the alloy is single-phase β (*i.e.*, the beta transus, or T_β) play an important role in selecting TMP parameters.

From a metallurgical standpoint, TMP of α/β *titanium alloys* is controlled to convert a coarse (multi-millimeter) structure of β grains (containing colonies of α lamellae) into one comprising fine, uniform, equiaxed α in a matrix of transformed β (Figure 1). For this purpose, ingots are first synthesized *via* processes such as vacuum-arc and cold-hearth (electron-beam or plasma) melting yielding a macrostructure comprising large columnar β grains with fine, free-surface and

S.L. SEMIATIN is with the Air Force Research Laboratory, Materials and Manufacturing Directorate, AFRL/RXCM, Wright-Patterson Air Force Base, OH 45433-7817. Contact e-mail: sheldon.semiatin.1@us.af.mil
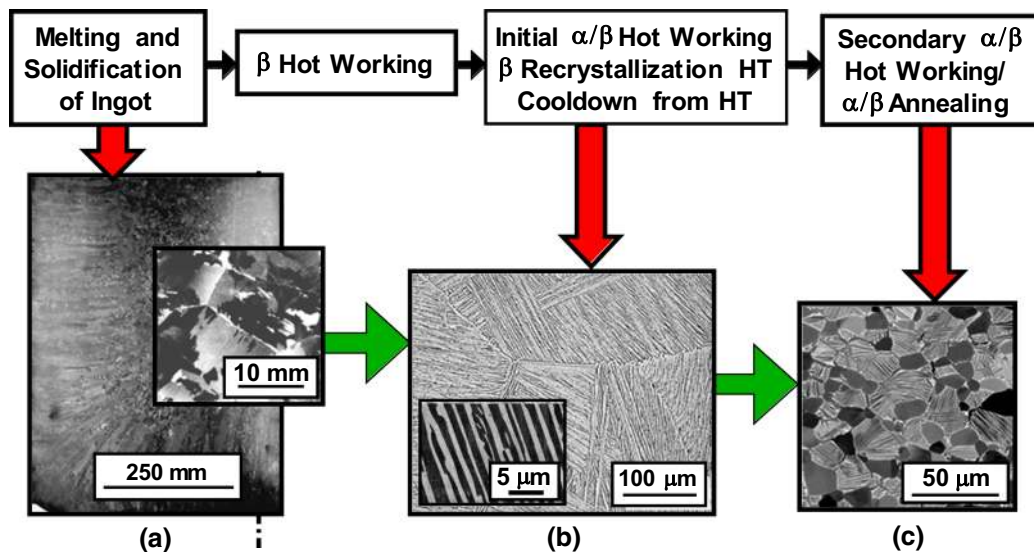
Fig. 1—Illustration of microstructure evolution during the TMP of α/β titanium alloys: (a) Macrostructure and microstructure of as-cast ingot, (b) microstructure after β recrystallization, and (c) microstructure after spheroidization of lamellar-α microstructure via α/β hot working.

coarser-interior equiaxed-β grains (Figure 1(a)). During slow cooling following solidification, the β phase within each grain transforms into lamellar colonies of alpha platelets. Primary processing consisting of deformation in the β field and then α + β field followed by additional hot work and/or heat treatment in the β field is applied to recrystallize the β grains to a size of the order of 0.5 to 2 mm (Figure 1(b)). Subsequent deformation and heat treatment in the α + β field is applied to spheroidize the colony microstructure within each β grain to obtain a microduplex structure of primary α particles (present at the hot-working temperature) in a matrix of β grains/subgrains each of which have transformed to produce colonies of so-called secondary-α plates (developed during slow cooling) or Widmanstatten-α laths (developed during fast cooling) (Figure 1(c)). Typical mill products made by these methods include billets, plate, and sheet.

The microstructure and crystallographic texture developed during mill processing can undergo further changes during part processing via methods such as open- or closed-die forging, isothermal or hot die forging, forward or backward extrusion, ring rolling, superplastic sheet forming, and various final heat treatment operations. In such cases, process parameters are selected to limit the coarsening of primary α, to control the volume fractions of primary and secondary α, and establish desirable deformation and transformation textures for alloys which are processed below T_β, i.e., at a subtransus temperature. Alternatively, control of the β grain size/shape and the nature of the α lamellae/laths formed during cooling are of prime interest for components which are forged and/or heat treated above T_β.

Some of the key considerations regarding deformation, microstructure evolution, and defect formation during various stages of the TMP of α/β and near-α titanium alloys (and, in some respects, the early/ingot-breakdown stages for β titanium alloys) are summarized in Figure 2. Although these phenomena are interrelated, the current understanding, outstanding questions, and research opportunities related to each are discussed in separate sections below. The reader is also referred to various books,[1,2] review papers related to TMP of titanium alloys,[3–9] as well as the proceedings of the quadrennial World Titanium Conferences, the latest of which was held in Nantes, France in June 2019. Research in this area has expanded significantly during the last two decades. Hence, the discussion below is aimed at providing a flavor of the status and needs and does not purport to be an exhaustive survey of the literature.

II. HOT DEFORMATION

In this section, hot deformation behavior in terms of slip systems, plastic flow observations, dynamic restorative processes, and constitutive models for α/β titanium alloys are summarized for the each of the phases as well as aggregates containing both phases. Much of the discussion refers to common alloys such as Ti-6Al-4V and Ti-6Al-2Sn-4Zr-2Mo-0.1Si (weight percent), hereafter referred to as Ti64 and Ti6242, respectively.

A. Deformation Mechanisms

By and large, slip processes within the α and β phases (and across α/β interfaces) accommodate imposed deformation at hot-working temperatures and

Melting and Solidification of Ingot

- Melt loss/composition/ segregation control
- Micro-porosity evolution
- β solidification texture
- β grain structure/ nonuniformity

β Hot Working

- β slip systems
- β texture evolution
- Strain-induced porosity (SIP)
- Uniformity of hot working

Initial α/β Hot Working β Recrystallization HT Cooldown from HT

- Static recrystallization of β/ β texture evolution
- β grain growth/β texture evolution
- Transformed microstructure formed on cooling
  - α variant selection
  - α platelet thickness

Secondary α/β Hot Working

- Coarsening of lamellar α
- Plastic flow/deformation mechanisms of two-phase microstructure
- Spheroidization: Dynamic Static
- Texture/microtexture evolution for α and β phases
- Coarsening of primary α
- Strain-induced porosity (SIP) (cavity initiation, growth, coalescence; cavity sealing)

Secondary Forming -Forging -Superplastic Forming - etc.

- Primary α coarsening at forming temperature
- Strain distribution
- α and β phases-texture evolution during hot working
- Secondary-α variant selection on cooling
- Interaction of microstructure and composition for superplastic deformation
- Microstructure evolution during transient phenomena (e.g.,solid-state joining)

Final Heat Treatment

α/β Heat Treat (e.g., engine parts)
- Primary α coarsening at T_p
- Primary α growth/ secondary α formation during cooling
- α variants formed in β

β Heat Treat (e.g., airframe parts)
- β grain growth
- Abnormal beta grain growth
- β texture evolution
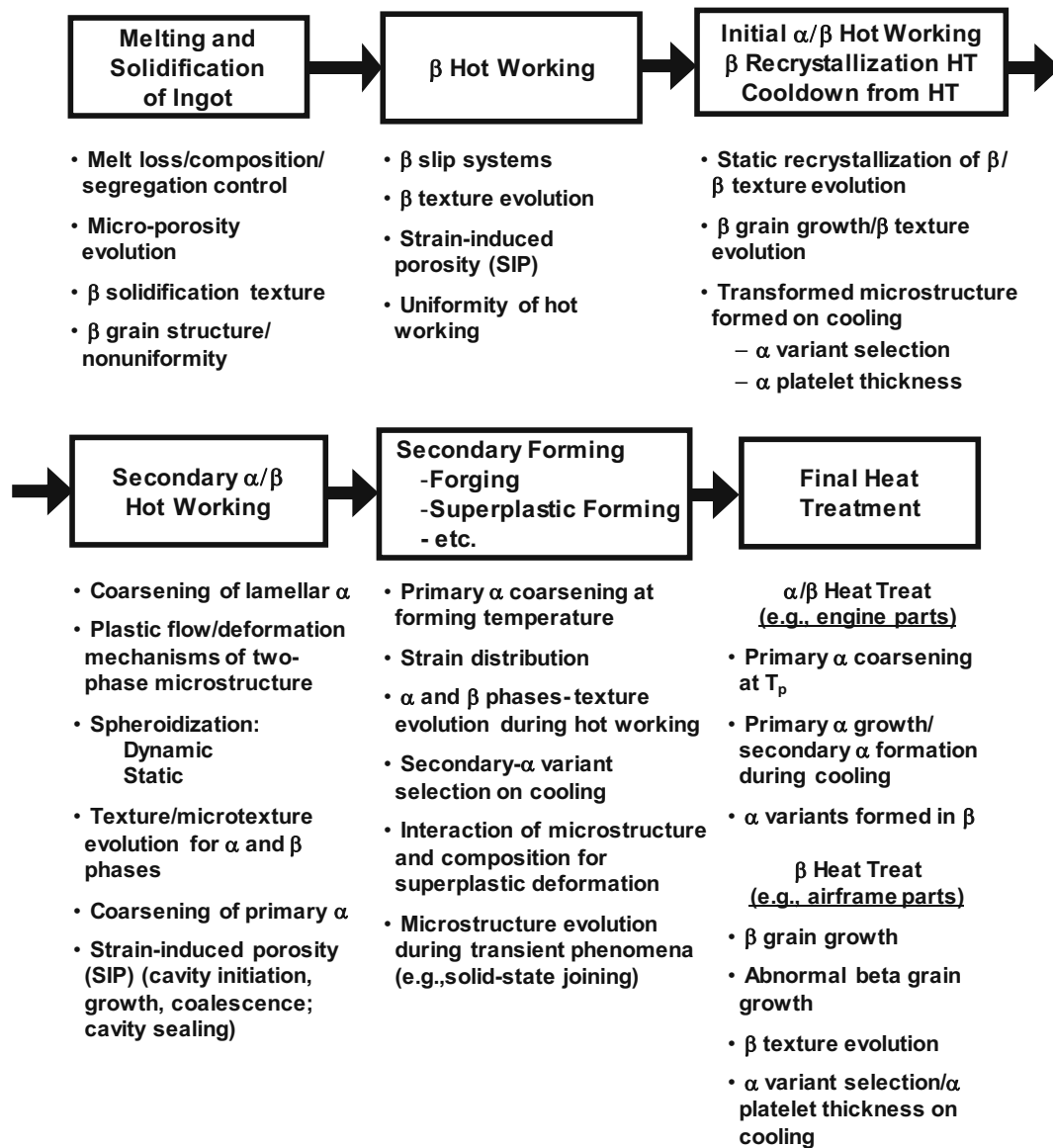- α variant selection/α platelet thickness on cooling

Fig. 2—Key steps in the TMP of α/β titanium alloys and associated deformation and microstructure-evolution phenomena.

conventional metalworking strain rates, *i.e.*, rates in the range of 0.01 to 250 s^{-1}. For processing under such conditions, there are very few direct measurements of the critical resolved shear stress (CRSS) and slip systems.[10] Rather, such information has been typically inferred from lower-temperature measurements, *e.g.*, Reference 11, or parametric crystal-plasticity simulations using various combinations of slip systems and relative values of CRSS which are tuned to provide agreement with measurements of flow-stress anisotropy (in textured materials) or the evolution of deformation texture. The latter method has been applied to the deformation of single-phase β above T_β[12,13] as well as α/β Ti alloys with an equiaxed- or colony-α microstructure below T_β.[14,15] This work has shown that the deformation of the β phase in α/β titanium alloys can be described by slip along ⟨111⟩ directions lying in {110}, {112}, or {123} planes, each with a CRSS which is typically ~1/3 of that for prism ⟨a⟩ slip in the α phase in these materials. Correspondingly, the ratio of the CRSSs in the α phase are approximately 1:1:1.5:3 for prism ⟨a⟩, pyramidal ⟨a⟩, basal ⟨a⟩, pyramidal ⟨c + a⟩ slip systems.[14,15] Due to the presence of thin layers of β, slip behavior for the α phase in α/β titanium alloys with a colony-α microstructure is even more anisotropic than that in aggregates of equiaxed-α grains. In such cases, the presence or absence of a co-linear ⟨a⟩ direction in α and ⟨111⟩ in β gives rise to prism ⟨a⟩ and basal ⟨a⟩ systems which are softer or harder, respectively.[10]

As for various metals which undergo superplastic flow at low strain rates (typically ≤ 0.01 s^{-1}), the majority of hot deformation imposed at such rates on α/β titanium alloys with fine, equiaxed-α microstructures is accommodated by sliding along α/β interfaces.[16–20] The stress concentrations developed at triple points during such sliding is accommodated by slip in the two phases.

B. Plastic Flow and Dynamic Restorative Mechanisms

Under hot-working conditions, the plastic flow (stress-strain) response of the individual α and β phases in α/β titanium alloys typically exhibits an initial strain-hardening region, a peak flow stress, and then steady-state flow or very gradual flow softening/hardening. Example flow curves for two single-phase α alloys and for Ti6242 in the single-phase β field (i.e., at 1283 K (1010 °C) are shown in Figure 3; the composition Ti-6.9Al-1.6V (weight percent) approximates that of the α phase in Ti64 at hot-working temperatures.

Additional examples for single-phase α alloys, single-phase β alloys, and α/β alloys tested above T_β are summarized in References 5, 6, and 21 through 29. From a broad perspective, the shapes of such curves result from the competition between strain hardening due to dislocation multiplication and the annihilation of dislocations due to dynamic recovery and boundary migration, i.e., continuous dynamic recrystallization.[25–27,29,30] Discussed in more detail in Section II, substructures associated with these mechanisms typically comprise subgrains within prior grains and mobile and immobile dislocations. At strain rates less than or equal to ~ 0.01 s^{-1}, the flow curves of β titanium alloys may also show a yield point associated with strain aging.[5]

During deformation at subtransus temperatures (i.e., in the $\alpha + \beta$ phase field), the shapes of the flow curves of α/β titanium alloys having a starting microstructure of equiaxed α in a matrix of β are similar to those of the single-phase alloys[21,23,26,31,32] (e.g., Figure 3(b)). As for single-phase β titanium alloys, α/β alloys with an equiaxed-α microstructure may also exhibit a yield point associated with strain aging at low strain rates.[33] By contrast, the subtransus flow curves for α/β titanium alloys with a starting "transformed" microstructure of lamellar/colony α or basketweave/Widmanstatten α exhibit a short strain-hardening region, a usually-sharp (well-defined) peak stress, and then noticeable flow softening[15,21,34–39] (e.g., the results in Figure 4). Because the lamellar/lath α phase is relatively thin (typically ≤ 2 μm), the formation of equiaxed cells/subgrains (due to dynamic recovery) is restrained, and the overall rate of hardening at low strains (≤ 0.05) tends to be higher for transformed microstructures.

Furthermore, due to Hall–Petch-like effects,[36] the low-strain (peak) stresses are often considerably higher than those for initial microstructures comprising equiaxed α in a β matrix deformed at the same temperature and strain rate.

The high flow-softening rates at low strains for α/β titanium alloys with an initial transformed microstructure have been variously attributed to dynamic spheroidization (often referred to as dynamic "globularization" in industrial practice), changes in crystallographic texture, etc. Because the majority of dynamic spheroidization occurs at strains in excess of ~ 0.5,[34,35] observed softening observations cannot be correlated to it. Secondly, it has been suggested that texture changes associated with the rotation of α platelets to soft orientations during compression can be used to explain a majority of the flow softening.[40] However, measured softening rates in compression and tension have been found to be similar[41]; and the difference in such cases has been ascribed to differences in texture evolution.[42] An additional possible explanation for the flow-softening phenomenon was established by hot compression tests on Ti64 samples having transformed microstructures consisting of lamellae with different thicknesses, but with the same overall texture.[36] By this means, it was surmised that slip transfer across α/β interfaces and the concomitant loss of Hall–Petch-like strengthening
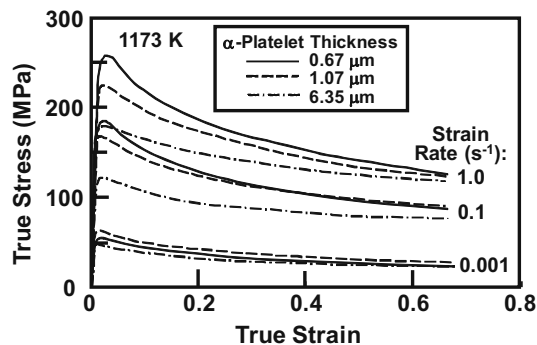

Fig. 4—Flow curves for Ti64 with a colony- or Widmanstatten-α microstructure having various α-platelet thicknesses.[36]
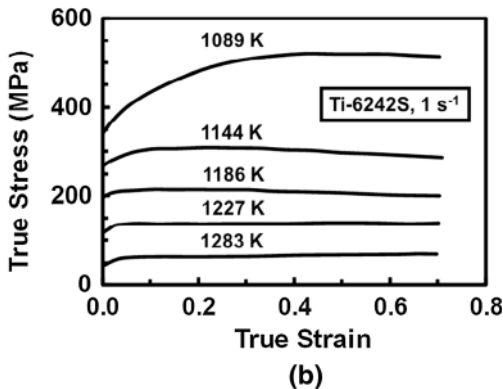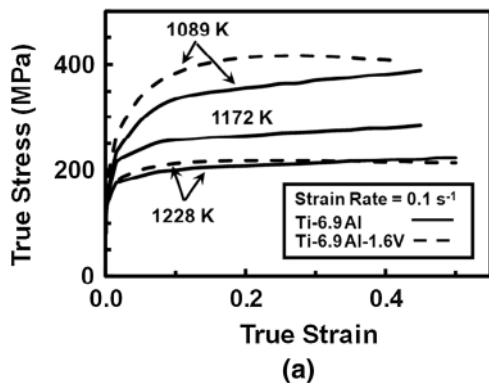

Fig. 3—Deformation-heating-corrected flow curves for (a) the single-phase α alloys Ti-6.9Al and Ti-6.9Al-1.6V and (b) Ti6242 in the $\alpha + \beta$ phase field [T $\leq$ 1227 K (954 °C) or β field [T = 1283 K (1010 °C)].[21] All alloys had an equiaxed-α starting microstructure.

with increasing strain may be an important source of flow softening in α/β titanium alloys with a colony- or Widmanstatten-α microstructure.

C. Constitutive Modeling

The constitutive modeling of the plastic flow of α/β titanium alloys has been largely phenomenological in nature with a few investigations involving the development of internal-state variable descriptions, the latter mostly for the single-phase constituents.

1. Phenomenological models

Because plastic flow of metals is usually thermally activated, engineering constitutive relations for titanium alloys have often comprised fits of measured initial (or steady-state) flow stress σ as a function of the Zener-Hollomon parameter $Z = \dot{\varepsilon}\exp(Q/RT)$ in which $\dot{\varepsilon}$ and T are the imposed strain rate and test temperature, respectively. Under conventional hot-working conditions, $\sigma^n \sim Z$, in which n is the stress exponent. This expression can then be rewritten as the following

$$\sigma = C\dot{\varepsilon}^m \exp\left(\frac{mQ}{RT}\right) = k(T)\dot{\varepsilon}^m \qquad [1]$$

Here, C is a constant, m is the strain-rate sensitivity ($= 1/n$), Q is an apparent activation energy for the micromechanical processes that control plastic flow, and R is the gas constant. Values of Q for *single-phase α* alloys are generally in the rage of 200 to 300 kJ/mol,[6,43,44] and those for deformation in the *single-phase β* field are usually between 150 and 200 kJ/mol.[5,22,23,45,46] The magnitude of m is usually in the range of 0.2 to 0.33 with the specific values for the β phase being comparable to or slightly higher than those for the α phase.

A number of investigators have also attempted to fit flow stress data measured in the *two-phase α/β* field to a constitutive relation of the form of Eq. [1]. In so doing, apparent activation energies in the range of 300 to 450 kJ/mol (for equiaxed-α microstructures) or 320 to 500 kJ/mol (for colony/Widmanstatten-α) have usually been obtained for alloys such as Ti64, Ti6242, and Ti17.[23,31,37,47]

The common observation of noticeable differences between the magnitude of Q for the deformation of two-phase alloys (such as α/β titanium alloys) compared to those for the corresponding single-phase materials has been explained in the context of variations in phase volume fractions with temperature for the former materials.[48] To quantify this behavior, three different flow-stress models were developed in Reference 48: (1) An upper bound model (assuming identical strains/strain rates in the two phases), (2) a lower bound model (assuming identical stresses), and (3) a continuum self-consistent (SC) model for the specific case in which the strain rate sensitivities of the two (assumed equiaxed) phases are identical. The SC model ensures that the macroscopic stress and strain are rule-of-mixtures averages of the different stresses and strains/strain

rates generated in each phase. Analytical expressions were derived for both the isostrain and isostress approaches. For the isostrain model, for example, the following relation was obtained:

$$Q = \frac{f_\alpha\sigma_\alpha m_\alpha Q_\alpha + (1-f_\alpha)\sigma_\beta m_\beta Q_\beta}{f_\alpha\sigma_\alpha m_\alpha + (1-f_\alpha)\sigma_\beta m_\beta} - RT^2\frac{(\sigma_\alpha - \sigma_\beta)}{m\sigma}\frac{df_\alpha}{dT} \qquad [2]$$

In Eq. [2], f_α is the volume fraction of α, and the stress, strain rate sensitivity, and activation energy of each phase is denoted by the corresponding subscripts. The aggregate flow stress (σ) is the volume-fraction-weighted average of the flow stress in each phase, and the aggregate rate sensitivity (m) is the average of that of each phase weighted by $f_i\sigma_i$ ($i = \alpha, \beta$). Eq. [2] also reveals that the overall activation energy Q is a function of the temperature dependence of the phase fractions, as quantified by the second ("mechanical-contribution") term on the right-hand side. A similar expression was derived for the isostress case. The SC approach yielded a numerical method to estimate the aggregate flow stress as a function of temperature from which the apparent activation energy can be derived.

The SC technique formulated in Reference 48 has been applied several times in the literature to predict the (low-strain/peak) flow stress of α/β titanium alloys (such as Ti64 and Ti6242) with an equiaxed-α microstructure during hot working in the two-phase field at conventional strain rates.[49–51] For this purpose, the flow stress of the individual α and β phases (with compositions identical to those of the phases in the two-phase alloys) were estimated from data for binary alloys[43–46] and solid-solution-strengthening effects based on an aluminum equivalent (for α) and a vanadium equivalent (for the β phase). The activation energies for plastic flow of single-phase α and β were taken to be 273 and 160 kJ/mol, respectively. A comparison of measurements and predictions of the flow stress of Ti64 at 0.1 s^{-1} is summarized in Figure 5(a).[15,49,52–54] The corresponding plot of $\ln\sigma$ vs $1/T$ (Figure 5(b)) yielded an apparent activation energy of 445 kJ/mol, in agreement with previous measurements.

The SC approach has also been applied to derive nomograms of the aggregate strength coefficient (k in Eq. [1]) as a function of the strength coefficient for each of the two phases (k_1, k_2) and the volume fraction of the harder phase (f_1) for various rate sensitivities. An example of such calculations for $m_1 = m_2 = m = 0.23$ (comparable to that for α/β titanium alloys at hot-working temperatures) is given in Figure 6. Among other applications, such nomograms can provide broad insight into plastic flow behavior for lots of material which exhibit various crystallographic textures that lead to variations in the strength-coefficient ratio ($k_1 : k_2$).

Continuum SC models also provide useful insight into the effect of local orientation on observations of non-uniformity in spheroidization and cavity formation during the hot working of α/β titanium alloys with a lamellar microstructure. Discussed further in Sections III and IV, respectively, the deformation of α colonies is
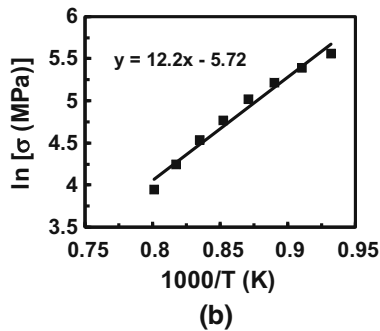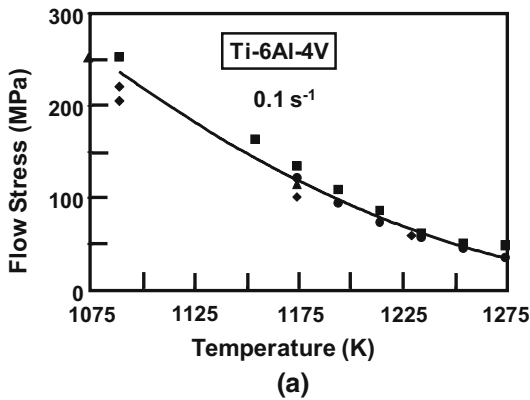
Fig. 5—Self-consistent model predictions for the flow stress of Ti64 at hot-working temperatures and a strain rate of 0.1 s^{-1}: (a) Comparison of predictions and measurements in the literature[49] and (b) Arrhenius plot to determine the activation energy.

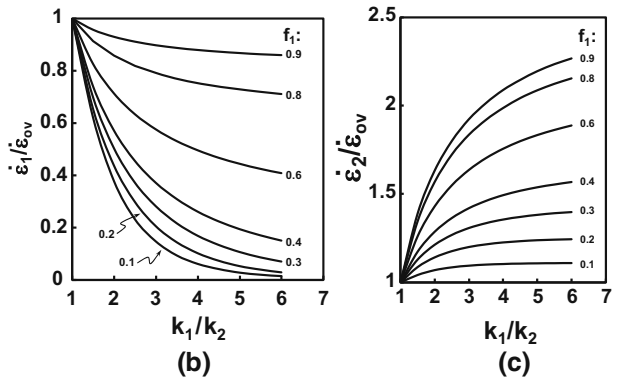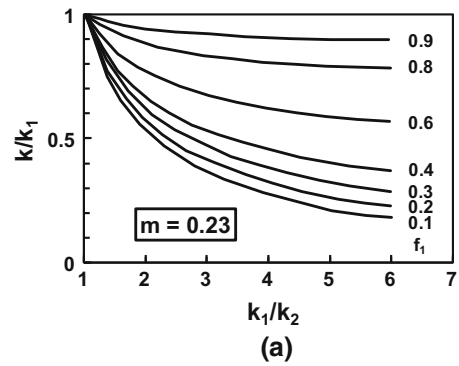

Fig. 6—Nomograms to determine (a) the strength coefficient k for an aggregate of two phases and (b, c) the ratios of the strain rates in the harder ("1") and softer ("2") phases to the overall strain rate as functions of the individual strength coefficients (k$_1$ and k$_2$) and the volume fraction of the harder phase (f$_1$), assuming m$_1$ = m$_2$ = m = 0.23.[49]

treated in such instances in a "homogenized" fashion. Unfortunately, there have been very limited attempts to apply a SC approach to model the constitutive behavior of titanium alloys with a lamellar microstructure for which the deformation in each phase is treated separately. An exception is the work of Canova and Lebensohn.[55] However, slip transmission across α/β interfaces was not taken into account in their approach.

The presence of two-phases can also present challenges with respect to the constitutive modeling of low-strain-rate superplastic deformation of α/β titanium alloys with fine, equiaxed microstructures. Most of these analyses are based on the classical Bird-Mukherjee-Dorn relation[56,57] for *single-phase alloys*:

$$\dot{\varepsilon} = \left(\frac{ADGb}{kT}\right)\left(\frac{\sigma}{G}\right)^n \left(\frac{b}{d}\right)^p \quad [3]$$

In this equation, A is a constant, D is a diffusivity, k is Boltzmann's constant, T is absolute temperature, G is the shear modulus, b is the length of the Burgers vector, n is the stress exponent of the strain rate (as above), and p is the grain size exponent of the strain rate. For superplastic deformation characterized by grain-boundary sliding (gbs) accommodated by climb/glide of dislocations, n ~ 2 and p ~ 2. For gbs accommodated by diffusional flow, n ~ 1 and p ~ 2 or 3, depending on whether bulk (lattice) or boundary diffusion predominates.

The application of Eq. [3] for two-phase materials such as α/β titanium alloys can be problematical because of ambiguity as to which phase the values of D, G, b, and d relate and the strain and/or stress borne by each phase. It is often assumed that d is the size of the alpha particles, and D is the diffusivity of substitutional solutes within the β phase or along α/β interfaces; isostrain or isostress behavior of the two phases has also been postulated.[16–19,58] For cases in which the equilibrium subgrain size for the α-phase *exceeds* its particle size (*e.g.*, in ultrafine materials), it has been shown that the deformation of Ti64 is accommodated largely by interface sliding.[58] In these instances, superplastic flow in the strain rate range of 0.0001 to 0.001 s^{-1} can be modeled over a relatively-wide temperature range (923 K to 1255 K, or 650 °C to 982 °C) using Equation [3] in which d pertains to α, and D, G, and b to β[20,59] (Figure 7). The apparent activation energy deduced from the plot in Figure 7 (160 kJ/mol) is identical to the direct measurement of Oikawa, *et al.*[45,46] for β titanium alloys as well as that used above for the β phase in the SC analysis of plastic flow in the two-phase field at *conventional* strain rates (> 0.01 s^{-1}). Thus, it can be inferred that plastic flow in the β phase serves to accommodate stress concentrations developed due to sliding along α/β interfaces during superplastic deformation.
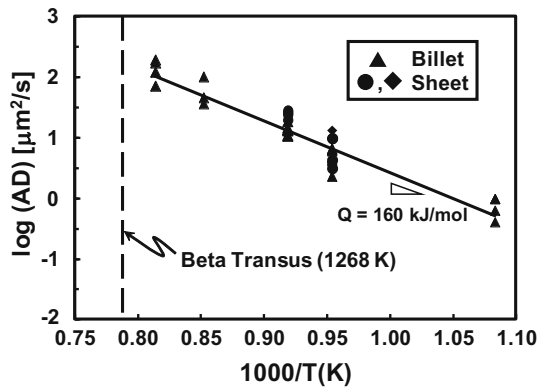
Fig. 7—Plot of log (AD) versus 1000/T for Ti64 with an ultrafine microstructure deformed under superplastic conditions.[20,59]

2. Internal state variable models

Internal state variable (ISV) models to predict the plastic-flow behavior of α/β titanium alloys have focused on the hot deformation of single-phase β as well as two-phase aggregates. Those for single-phase β have been of two types: single variable (mobile dislocation density) and higher-order approaches which include multiple variables (e.g., mobile and immobile dislocations, low-angle boundaries, high-angle boundaries).

Single-variable models[25,60–62] describe the competition between the generation and annihilation of dislocations whose density is denoted as ρ, i.e.,

$$d\rho/d\varepsilon = (\partial\rho/\partial\varepsilon)^{+} - (\partial\rho/\partial\varepsilon)^{-} \qquad [4]$$

For the Laasroui and Jonas,[60] Montheill et al.,[61] and Kocks and Mecking[62] formalisms, respectively, Eq. [4] becomes the following:

$$d\rho/d\varepsilon = h - r\rho \qquad [5a]$$

$$d\rho/d\varepsilon = H^{\nu+1}/\rho^{\nu} \qquad [5b]$$

$$d\rho/d\varepsilon = k_3\rho^{0.5} - k_4\rho \qquad [5c]$$

Here, h/r, H/ν, and k_3/k_4 denote the hardening and softening parameters in the three different approaches. In each case, the flow stress σ is assumed to be a function of the dislocation density per the classical Taylor relation, $\sigma = aGb\rho^{0.5}$, in which a is a constant usually between 0.5 and 1. Integrating Eq. [5a] and inserting this relation yields the final result for the Laasroui-and-Jonas formulation[60]:

$$\sigma = \left[\sigma_o^2 \exp(-r\varepsilon) + aGb(h/r)(1 - \exp(-r\varepsilon))\right]^{0.5} \qquad [6]$$

The term σ_o is the yield stress, and the steady-state stress σ_{ss} is given by the following:

$$\sigma_{ss} = aGb(h/r)^{0.5} \qquad [7]$$

Expressions such as Eq. [5a] (and the corresponding flow stress dependence on strain) may be further modified by adding a term to account for the annihilation of dislocations by the migration of sub-boundaries.[25] These equations have been used to predict the flow stress of Ti64 in the β field and Ti64 and Ti17 (and other alloys) in the $\alpha + \beta$ field.[24,25,38,63,64]

More advanced ISV models have also been developed.[26,27,29,39,65–67] In addition to mobile dislocation density, these approaches consider other factors such as cell/subgrain size (associated with geometrically-necessary dislocation content), grain size (i.e., high-angle-boundaries), and immobile dislocation content. By this means, the plastic flow of Ti64 and Ti17 in the single-phase β field have been simulated.[27,29]

D. Future Research Opportunities

A number of challenges related to the hot deformation of α/β titanium alloys remain and present opportunities for future research, including the following:

- Plastic flow of single-phase α: Compared to measurements and ISV models for the hot deformation of α/β titanium alloys in the single-phase β field, there appears to be a dearth of similar information for single-phase-α alloys with compositions corresponding to those of the α phase in these materials. As mentioned previously, much of the existing literature pertains to binary (Ti-Al) alloys.[43,44] Additional measurements and interpretation for Ti-Al-X compositions (X = V, Mo, Sn, Zr, etc.) processed under hot-working conditions would be useful.

- Strain-partitioning during plastic flow: With the increasing availability of high-energy synchrotron sources and high-speed X-ray detectors, the effect of local texture, phase fractions, etc. on the partitioning of strain between the α and β phases during hot working can be quantified. Such information would be useful to calibrate both simple constitutive models as well as advanced crystal-plasticity codes employed to simulate the evolution of deformation textures.

- Plastic flow of α/β titanium alloys with a colony-α microstructure: Measured flow stresses for poly-colony samples of α/β titanium alloys represent the average response of the aggregate and not the properties of specific activated slip systems. Measurements of the behavior of single colonies of α/β titanium alloys that would complement those in Reference 10 (for which the α-platelet thickness was ~8.5 μm) should be made as a function of strain rate, temperature, α-platelet thickness, etc. It would be especially useful to evaluate samples with α-platelets whose thickness is much less than the equilibrium subgrain size at typical hot working temperatures and strain rates, i.e., less than ~5 μm. Such thicknesses would mirror those typically developed in (polycolony) mill products, i.e., ~2 μm.

- Plastic flow of α/β titanium alloys under transient-temperature conditions: The TMP (and solid-state joining) of α/β titanium alloys often involves temperature transients. These transients can include temperature decreases (*e.g.*, due to die chill during conventional hot forging, roll chill during plate/sheet rolling, water quenching, *etc.*) and temperature increases (*e.g.*, due to deformation or frictional heating), either of which can result in the retention of a metastable microstructure, phase composition (especially in the β phase), or both. Such effects on plastic-flow behavior have been documented and interpreted to only a limited extent in the literature, *e.g.*, References 49, 68 through 70, and thus warrant further investigation.

III. MICROSTRUCTURE EVOLUTION

During TMP, α/β titanium alloys undergo a wide variety of microstructural changes, each with its associated driving forces. For processing in the single-phase β field, these changes include CDRX (and sometimes discontinuous dynamic recrystallization, or DDRX), static recrystallization, and grain growth. In the two-phase α/β field, coarsening of lamellar or equiaxed α, substructure formation and dynamic/static spheroidization of lamellar/Widmanstatten α, and the development of various deformation and transformation textures are important.

A. *CDRX During β Hot Working*

Microstructure evolution during hot working of α/β (and β) titanium alloys in the β field is usually controlled by dynamic recovery/CDRX, comprising the formation of subgrains whose misorientations tend to increase with strain.[71,72] For coarse-β-grain starting structures typical of that encountered in production-scale ingots, however, deformation is usually non-uniform, being greater at and near the original grain boundaries and less near the center of the grains. In addition to non-uniform subgrain structures, the higher deformation at the β grain boundaries also tends to lead to the generation of a "necklace" layer of very fine grains; it has been suggested that such grains form by DDRX.[23,73,74] For alloys such as Ti64 and Ti834 deformed at low supertransus temperatures (~15 to 50 K, or 15 to 50 °C, above T_β), the volume fraction of DDRX grains is typically small (≤15 pct.). These trends can be more readily discerned following β hot working of near-β and β titanium alloys for which phase decomposition during cooling is avoided or retarded, thus enabling retention of the high-temperature microstructure.[5,71,72,75–77] For example, OuYang et al.[77] have shown that large strains (of the order of 2) must be imposed at low strain rates (0.01 s^{-1}) and high temperatures relative to T_β to bring about a microstructure that is fully refined *via* DDRX in Ti-10V-2Fe-3Al.

The evolution of subgrain structures during hot working of α/β titanium alloys in the β phase field has been quantified experimentally (using electron backscatter diffraction (EBSD) techniques) and theoretically (*via* mesoscale modeling approaches). For example, Poletti et al.[26] measured the subgrain size (D) developed during hot working of Ti64 in the β field and related it to the steady-state flow stress (σ_{ss}) using the classical relation due to Derby,[78] *viz.*,

$$\sigma_{SS}/G = K(D/b)^{-p} \qquad [8]$$

in which G and b have the same meaning as for Eq. [3], p is a positive, material-independent constant (typically equal to 2/3 for DDRX grains and 1 for CDRX grains/subgrains), and K is a material constant between 1 and 10. For Ti64, Poletti et al.[26] found experimentally that p and K were equal to 0.64 and 3.42, respectively. Similar values of p and K (0.68 and 0.83, respectively) were derived when the analysis of the experimental data was done in terms of the stress *increment* due solely to the subgrains as distinct from the influence of the matrix (friction) stress.

Similar EBSD measurements of grain/subgrain sizes developed during hot working in the β field of Ti64 and the β alloys Ti-15V-3Cr-3Sn-3Al and Ti-10V-2Fe-3Al were performed by Seshacharyulu[79] and Furuhara et al.,[76] respectively. In both efforts, it was found that the size was linearly dependent on the Zener-Hollomon parameter Z, with a slope of -q, when plotted on a log-log scale. Assuming that $\sigma^n \sim Z$, in which n denotes the stress exponent as above, this dependence can be written alternatively as the following:

$$\log D = -q \log Z + C_1, \qquad [9a]$$

$$\text{or,} \quad D\sigma^{n \cdot q} = 10^{C_1} \qquad [9b]$$

A comparison of Eqs. [9b] and [8] reveals that p = n·q. For Ti64, q was 0.17[79]; assuming n = 3, p = 0.51. For Ti-15V-3Cr-3Sn-3Al,[76] q for both DDRX grains and CDRX subgrains was 0.41. Taking n = 3, p would be 1.2. The value of q for the formation of DDRX grains in Ti-10V-2Fe-3Al[76] was 0.13, thereby yielding p = 0.39. Thus, it may be inferred the Derby relation may provide broad guidance on subgrain/grain formation during hot working in the β field, but alloy-dependent variations may be expected.

In addition to the modeling of flow curves described in Section II–C–2, mesoscale (ISV) models have also been successful in quantifying the details of subgrain/grain development during CDRX in the β field. In these instances, recovery-type processes result in the formation of sub-boundaries whose misorientations increase as additional dislocations are absorbed. The models can thus predict the evolution of subgrain size, misorientation distributions, *etc*. Results such as those in Figure 8 for Ti17[25] have revealed that strains of the order of 0.5 to 1 are required to achieve a steady-state subgrain size. The models also have indicated that the precise magnitude of the subgrain size is a strong
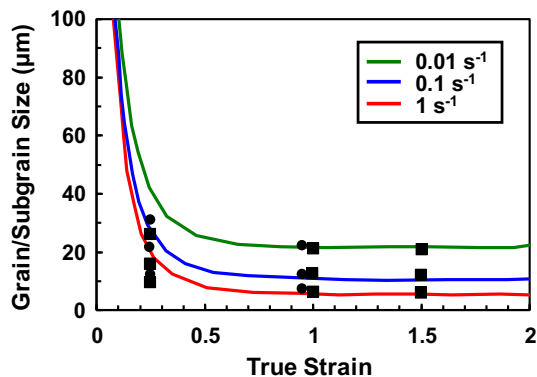
Fig. 8—Comparison of the measured evolution of subgrain size (data points) and internal-state-variable-model predictions (curves) for Ti17 hot worked in the β field (at 1183 K, or 910 °C) and the strain rates indicated.[25,80,81]

function of applied strain rate, in good agreement with experimental observations.[76,79–81] Recently, advanced mesoscale ISV models have been developed and applied for describing substructure evolution during β-field hot working of both Ti64 and Ti17.[27,29] These latter simulations provide additional insight into the evolution of not only subgrains but also the kinetics of the transition from subgrains to grains with high-angle boundaries. In particular, model predictions suggest that strains of the order of 0.5 to 1.5 or 2 to 3 are required to achieve a steady-state grain size during the hot working of Ti64 and Ti17, respectively, at a strain rate of 0.1 to 1 s^{-1} and a temperature ~70 to 90 K (70 to 90 °C) above T$_\beta$.

B. Static Recrystallization in the β Phase Field

Research on static recrystallization in the β phase field of α/β titanium alloys has focused on the influence of either β or α/β hot working prior to heat treatment.

1. Recrystallization following β hot working

Despite its industrial significance, relatively-limited work on β recrystallization following β hot working appears to have been published in the open literature.[81–83] Two related efforts[82,83] revealed the occurrence of a "critical grain growth" phenomenon in Ti64 and Ti-5Sn-0.5Mo. In both cases, small prestrains (less than approximately 0.05) resulted in little change in β grain size during subsequent supertransus annealing. For slightly higher strains (~0.05 to 0.10), substantially larger grain sizes were developed during annealing, i.e., ~600 → ~1700 μm for Ti64 and ~900→ ~1600 μm for Ti-5Sn-0.5Mo. For prestrains ≥ 0.1, the grain size after annealing exhibited an approximately exponential decay with increasing deformation. Nevertheless, the final annealed grain size was still slightly larger or slightly smaller than the starting grain size in Ti64 and Ti-5Sn-0.5Mo, respectively, for imposed strains as large as 0.7. The observations were explained in terms of heterogeneity in static recrystallization associated with variations in grain-to-grain deformation and accompanying variations in the rate of migration of the original high-angle boundaries.

The kinetics of static recrystallization of Ti64 during β annealing following β hot working have also been established.[84] For a prestrain of 1, the dependence of the fraction recrystallized X$_{SRX}$ on time t has been fit using the Avrami equation:

$$X_{SRX} = 1 - \exp[-(\ln2)(t/t_{0.5})^{n_a}]. \qquad [10]$$

Here, t$_{0.5}$ denotes the time for 50 pct. recrystallization, and n$_a$ is the Avrami exponent. In the work described in Reference 84, n$_a$ = 1 fit the measurements well, and t$_{0.5}$ decreased noticeably with increasing stored energy resulting from either higher imposed strains or strain rates. Overall, the values of t$_{0.5}$ were between ~60 to 240 s for prestrains of 1.0 to 0.4, respectively, imposed at a temperature 70 K (70 °C) above T$_\beta$. Similar values of t$_{0.5}$ were observed for samples of Ti834 which were hot worked to a strain of unity at T$_\beta$ + 55 K (T$_\beta$ + 55 °C) and then annealed at the same temperature.[74]

2. Recrystallization following α/β hot working

The application of a 15 to 30 pct. reduction during hot working at T$_\beta$ – 40 K (T$_\beta$ – 40 °C) of α/β titanium alloys with a colony-α microstructure is a common rule of thumb used in industrial practice to obtain a uniform, refined grain size during subsequent β annealing. Several investigations in the literature have provided a firm basis for this guideline by elucidating the quantitative effect of level of α/β prestrain, strain rate, etc. on β recrystallization of various alloys.[85–87] The early work of Elagina et al.[85] for alloys VT-3 (Ti-6Al-1.5Cr-2.5Mo-0.5Fe-0.3Si, T$_\beta$ ~ 1268 K, or 995 °C) and VT-9 (Ti-6Al-1.5Zr-3.5Mo-0.3Si, T$_\beta$ ~1243 K or 970 °C), for example, indicated that strains of the order of 0.1 to 0.2 could reduce the β grain size substantially (e.g., 7 mm → 0.5 mm for ingot products) during the early stages of annealing just above T$_\beta$ following hot working at T$_\beta$-75 K (T$_\beta$-75 °C). Only limited further refinement was obtained by using larger strains of ~0.5. In addition, the grain size refinement was found to decrease substantially if the prestrain was applied at a temperature close to T$_\beta$.

The interaction of static recrystallization and grain growth during β annealing following α/β hot working of alloys with a starting colony-α microstructure has also been quantified for α/β prestrains greater than or equal to ~0.25. Using prior-wrought material with a relatively-fine β grain size (~500 μm), Semblanet et al.[86] showed that recrystallization of Ti17, which results in grain-size refinement, requires relatively short times (≤ 30 minutes) and is followed by static grain growth, which can lead to β grain sizes comparable to or greater than the starting size. The importance of β-annealing time and temperature in controlling grain growth following recrystallization was also underscored in References 85 and 87. In particular, the use of direct-resistance heating (involving zero hold time) for β annealing, rather than furnace annealing, was employed to develop noticeably finer recrystallized β grain sizes.[85] In view of such findings, it may be surmised that β recrystallization

following small-strain α/β hot working may require only several, and not tens of, minutes.

The exact mechanisms of static recrystallization in the β field following *small levels* of α/β hot working of a colony-α microstructure remain unclear at present. Observations of recrystallization following *large α/β reductions* (corresponding to strains of ~1) of either a colony- or equiaxed-α microstructure do suggest, however, that the formation of a β microtexture either during prestraining or the early stages of recrystallization may play a key role.[25,88] Specifically, it has been shown that subgrains comprising the microtexture are consumed by a minor population of more-highly misoriented grains developed during hot working (Figure 9). In this regard, the mechanism appears to be analogous to *metadynamic* recrystallization[89] in which the nuclei (the more-highly misoriented grains) are formed during prior (α/β) hot working and then grow during subsequent (β) annealing. For the case of small prestrains applied to a colony-α starting microstructure, a similar mechanism may apply. In such instances, regions of locally-high deformation developed in the vicinity of β grain boundaries or lamellar kinks may give rise to the highly-misoriented grains that grow into the remaining, lightly-deformed, β matrix.
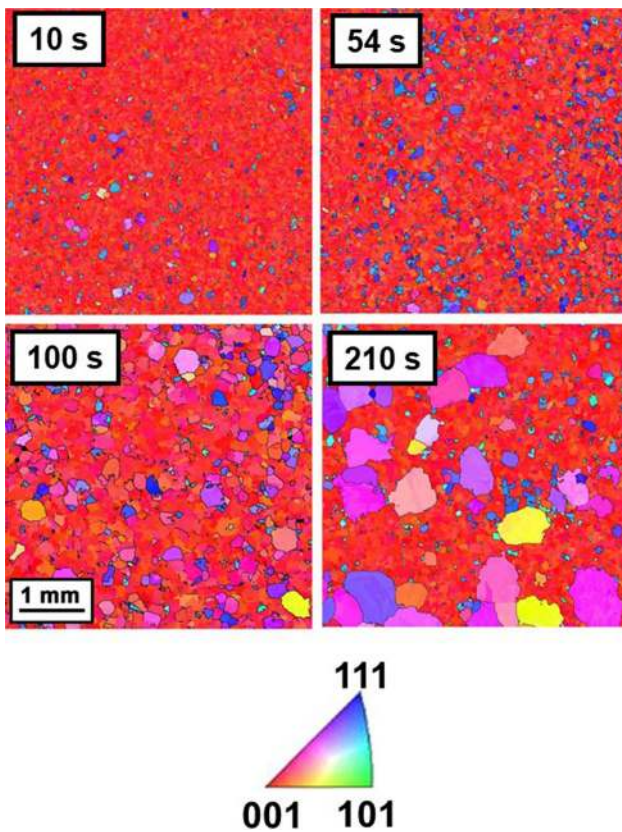

Fig. 9—Reconstructed, normal-direction inverse-pole figure maps for the β phase in a Ti64 sheet which was α/β rolled and then β annealed for the times indicated.[88]

C. *Static Grain Growth in the β Phase Field*

Static grain growth in the β phase field is of particular importance for α/β (and β) titanium alloys because of the effect of β grain size on subsequent processing (*e.g.*, α/β hot working to breakdown a transformed microstructure, the formation/retention/size of α-phase microtexture regions/macrozones) and service properties (*e.g.*, strength, ductility, dwell-fatigue behavior). Thus, considerable research has been performed to quantify and interpret β grain-growth kinetics.

Early efforts for α/β and near-α titanium alloys such as Ti64 and Ti685[82,89–91] revealed isothermal grain-growth behaviors which deviated from parabolic ("normal-growth") kinetics characterized by a growth exponent n_g of 2 in the phenomenological expression:

$$D^{n_g} - D_o^{n_g} = K_g(t - t_o) \exp\left(\frac{Q_g}{RT}\right) \qquad [11]$$

in which D and D_o are the grain size at time t and initial time t_o, K_g is the rate constant, and Q_g is the activation energy for grain growth. Rather, grain-size-vs-time plots indicated alternating periods of rapid and slow growth, and values of n_g between ~2 and ~6 that were a function of not only time but also temperature. Related observations[92,93] comprising continuous heating at a constant rate into the β phase field also suggested that a single set of material parameters (*i.e.*, n_g, K_g, and Q_g) could not be used to fit the measurements.

The source of the unusual behaviors was deduced to result from the evolution of texture during grain growth.[94,95] Specifically, texture evolution can lead to a temporal variation in the distribution of misorientations across beta grain boundaries and thus bring about concomitant variations in grain-boundary energy, mobility, and migration rates. In the simple case of a texture consisting of two components (A and B), each with its own spread, for example, the average growth rate would be expected to be either fast or slow when the volume fractions of components are either comparable or noticeably unequal, respectively. In the former instance, there would likely be a large fraction of high-mobility A-B grain boundaries. When the volume fractions are very unequal, there would be a large fraction of A-A or B-B boundaries having low mobility. Furthermore the alternating growth of one of the texture components at the expense of the other would lead to alternating cycles of fast and slow grain growth.

Attempts to simulate texture-controlled β grain growth for titanium alloys has led to the development of Monte-Carlo (Potts) models into which hypothetical or measured textures and grain-boundary properties can be instantiated.[96] Grain-growth simulations based of such formulations replicate the observations of fast and slow grain growth, a dependence of n_g on texture, *etc.*[96,97] However, quantitative agreement between observations and simulations is still lacking. One possible source of such differences is the input of improper material properties such as boundary energy/mobility as a function of either scalar misorientation or specific boundary plane. Until such properties are available, it is

not possible to ascertain the accuracy of Monte-Carlo (Potts) approaches *per se*. Similar remarks apply to other mesoscale approaches for simulating grain growth such as the phase-field method.[98]

D. *Lamellar-α: Nucleation, Growth, and Coarsening Phenomena*

The cooling rate following β annealing and reheat temperature/time during subtransus exposure have a major effect on the formation and coarsening of colony- or Widmanstatten-α and thus the kinetics of dynamic/static spheroidization during α/β hot working and final heat treatment of α/β titanium alloys. Descriptions of such phenomena have relied on both phenomenological and mesoscale-modeling approaches.

1. *Lamellae formation*
The formation of lamellar/acicular α has been addressed by Fox and Neal,[99] Gil *et al.*,[100] Malinov *et al.*,[101–103] and Wang *et al.*,[104] among others. For example, Fox and Neal[99] delineated the effect of cooling rate on the thickness of grain-boundary α (d_{gb}). This microstructural feature is difficult to eliminate during α/β hot working and can lead to losses in ductility and high-cycle-fatigue (HCF) resistance, especially for β titanium alloys.[105] Measurements showed that d_{gb} is related to the local cooling rate through the transus $(dT/dt)_\beta$ by an expression of the form:

$$(dT/dt)_\beta = A \exp(B d_{gb}) \qquad [12a]$$

$$\text{or} \quad d_{gb} = (1/B)\ln(dT/dt)_\beta - (1/B)\ln A \qquad [12b]$$

in which A and B are constants. A relation similar to Eq. [12b] can be fit to measurements by Gil *et al.*[100] of the thickness of colony-/basketweave-α platelets as a function of cooling rate and β-annealing temperature, the latter variable affecting the β grain size (Figure 10(a)). These thicknesses may be somewhat high, however, due to sectioning-plane (stereology) effects, preparation/imaging methods, *etc*.

In related work, Malinov *et al.*[101–103] applied a variety of techniques (*e.g.*, differential scanning calorimetry, resistivity, synchrotron X-ray diffraction) to measure the kinetics of the $\beta \rightarrow \alpha$ phase transformation for Ti64 and Ti6242. It was found that increasing cooling rate shifts α nucleation from a heterogeneous type at β grain boundaries to a homogeneous type within the grain interiors. The findings were modeled using a phenomenological (Johnson-Mehl-Avrami-Kolmogorov) approach as well as a finite-element technique in which the detailed nucleation and growth phenomena (N + G) were described. The latter provided insight in the spatial and temporal evolution of microstructure (*e.g.*, Figure 10(b)). A similar N + G approach has been developed to describe the decomposition of the β matrix to form lamellar α following solution treatment in the α/β phase field.[106]

The spatial evolution of the $\beta \rightarrow \alpha$ transformation was also quantified by Wang and his coworkers.[104]

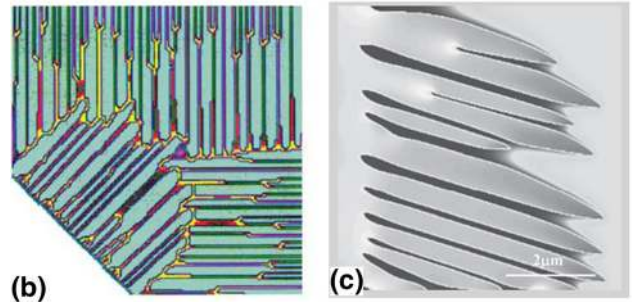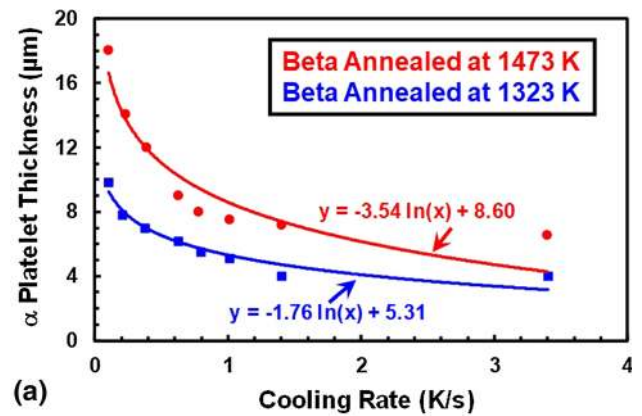Fig. 10—(*a*) Analytical fits (curves) to literature measurements (data points)[100] of the cooling-rate dependence of the thickness of colony-α platelets in Ti64 and (*b*), (*c*) example microstructure predictions for the formation of colony-α during the cooling of α/β titanium alloys obtained using (b) the finite-element method[103] and (c) the phase-field method.[104]

Assuming a morphological instability as the nucleation mechanism., they applied a two-dimensional phase-field method to simulate the growth and thickening of grain-boundary α and α sideplates which extend into the β matrix to form the colony structure (Figure 10(c)). The formation of basketweave-α *via* the nucleation and growth of sideplates from adjacent or opposite portions of the boundary of a given β grain was also simulated.

2. *Lamellae coarsening*
Due to the complex, three-dimensional geometry involved, the quantification of coarsening of α platelets during preheating prior to hot working is very challenging, both experimentally and theoretically. Experimental methods based on two-dimensional metallographic observations must rely on stereological corrections[107] or the artifice of using a specific sectioning plane deduced from prior processing.[108] Three-dimensional measurements, involving serial sectioning or synchrotron (X-ray) measurements, tend to be limited by the labor involved to obtain a statistically-meaningful dataset.[109–111]

Despite these difficulties, experimental observations have revealed that the early stages of lamellar coarsening (i.e., for times t<4h) comprise the elimination of individual "branches" attached to longer lamellae[112] (Figure 11). In this case, branch recession is governed by solute diffusion from the branch tip to the broad face of
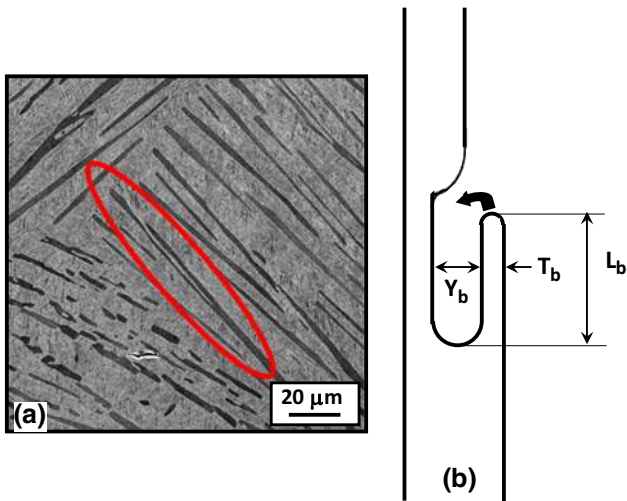
Fig. 11—Elimination of branches attached to α lamellae: (*a*) Example of a lamellar branch (circled) and (*b*) schematic illustration and nomenclature for analysis of branch recession.[112]

the adjacent lamella (Figure 11(b)). An analytical expression for the recession rate is readily derived by applying the Gibbs-Thompson equation for the concentration difference between the branch tip and adjacent (approximately flat) lamella, with the final result[112]:

$$\frac{dL_b}{dt} = \frac{\pi D C_F V_M \gamma_{\alpha\beta}}{R T T_b (Y_b + T_b/2)} \quad [13a]$$

in which

$$C_F = \frac{C_\beta (1 - C_\beta)}{(C_\alpha - C_\beta)^2 [1 + \partial \ln r / \partial \ln C_\beta]} \quad [13b]$$

Here, D is an effective diffusivity for the rate limiting solute, C_α, $C_\beta \equiv$ concentration of the rate-limiting solute in the α and β phases, respectively, $V_M \equiv$ molar volume of the α phase, $\gamma_{\alpha\beta} \equiv$ alpha/beta interface energy, R ≡ gas constant, T ≡ absolute temperature, and r ≡ activity coefficient of the rate-limiting solute in the β phase. The remaining geometry-related terms are defined in Figure 11(b).

The corresponding analysis of coarsening of a collection of lamellae at moderate-to-long times (t ≥ 4 h) is confounded by geometric complexity introduced by the plethora of possible spatial paths for solutes to diffuse from a given lamella tip to the broad face of a nearby (or its own) lamella. Thus, a general theoretical treatment does not appear to be tractable. Nevertheless, existing experimental data[35,113–115] suggest that the relationship between the average α-platelet thickness and time is parabolic in nature, *i.e.*, $d \sim t^{n_c}$, in which the coarsening exponent n_c lies in the range between 0.05 and 0.2 (Figure 12).

E. *Dynamic Spheroidization of α Lamellae*

The breakdown of α lamellae (or laths) during α/β hot working (*i.e.*, dynamically) or subsequent α/β annealing

(*i.e.*, statically) underlies the formation of the equiaxed-α microstructure. At typical hot-working temperatures, the equiaxed-α particles develop in a matrix of β grains. The surface tensions associated with triple points formed by α/β interfaces and β/β grain boundaries must balance. Thus, the α particles produced do not become spherical, but retain a globular shape. The conversion of a lamellar structure into an equiaxed one is therefore often referred to as "globularization". By analogy with other material systems, however, the terms spheroidization and globularization are frequently used interchangeably. In the subsections below, current understanding of the mechanisms of dynamic spheroidization and the overall kinetics are summarized.

1. *Mechanisms*

Early research by Margolin, Weiss, and their co-workers[116–119] demonstrated that hot working of α/β titanium alloys with a lamellar microstructure leads to the generation of high-angle α/α boundaries within the α platelets due to either shear localization or dynamic recovery (resulting in the formation of dense dislocation walls). The α/α boundaries lay normal to α/β interfaces and are spaced at periodic intervals within the α lamellae. (Similar features may also develop within the β interlayers.) If the strain is large enough, shear bands may be generated and result in fracture/segmentation of α lamellae. More frequently, the α/α interfaces within the α lamellae lead to surface-tension-driven penetration of the α plates by the β phase. (The splitting of β layers due to the generation of β/β boundaries and penetration of the α phase has also been observed, but is less frequent.) When this so-called boundary-splitting process, which results in the fragmentation of α lamellae, is controlled by bulk diffusion through the β matrix, the time to complete penetration (t_p) depends on the diffusivity of the rate-controlling solute (D), the ratio of the interfacial energies of α/α boundaries and the α/β interface ($\gamma_{\alpha\alpha}$ and $\gamma_{\alpha\beta}$, respectively), and the thickness of the α lamellae, d_α[120,121]:

$$t_p = \frac{0.2 R T d_\alpha^3}{D C_F V_M \gamma_{\alpha\beta} m^3} \quad [14a]$$

In Eq. [14a], C_F is the composition factor defined in Eq. [13b], m (= tan δ) is the groove slope (Figure 13), and the other symbols are the same as above. The relation between the groove geometry and the interface energies is given by the equilibrium equation, *i.e.*,

$$2\gamma_{\alpha\beta} \sin \delta = \gamma_{\alpha\alpha} \quad [14b]$$

Equation [14a] indicates a strong dependence of t_p on temperature (through the terms T and D), d_α, and the phase compositions (C_F term). Other less obvious dependences include those associated with strain rate (which determines the time for a given imposed deformation) and the evolution of dislocation substructure. At high strain rates and low temperatures, the time of deformation is short, and shear localization/fracture of lamellae may be favored over diffusion-controlled
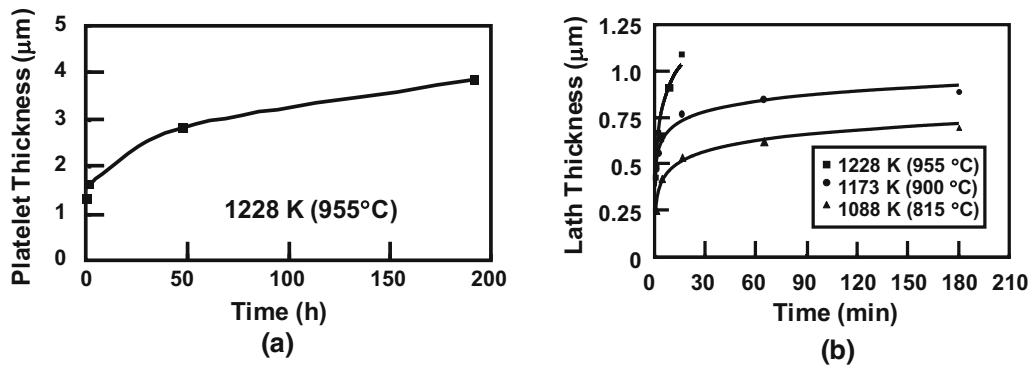
Fig. 12—Measured coarsening behavior of Ti64 with an initial microstructure of (*a*) lamellar (colony) α or (*b*) acicular (Widmanstatten) α.[35]
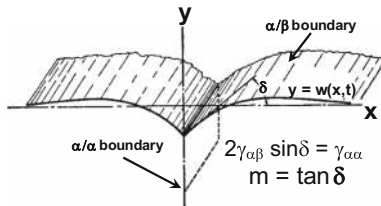

Fig. 13—Schematic illustration of the geometry during boundary grooving.[120,121]

boundary splitting. The development of dislocation substructure/sub-boundaries affects not only the evolution of the values of the interface energies themselves, but also the effective diffusivity of solutes through the β matrix. During deformation, the interface energies evolve with strain/time and therefore give rise to the common observation of a critical strain for the beginning of dynamic spheroidization.

A number of investigations of hot (and warm) working of α/β (and β) titanium alloys with a lamellar microstructure have verified the occurrence of the boundary-splitting mechanism and sought to quantify the evolution of sub-boundaries and the α/β interface energy.[76,122–131] For example, EBSD measurements have shown that the formation of sub-boundaries in α lamellae increases with strain.[76,123–125] In particular, sub-boundary misorientations of the order of 5° are developed after true strains of ~0.30 and increase to ~15° (or greater) by strains of ~1.1 - 1.3 in Ti64.[124,125] Furthermore, the *spacing* of the sub-boundaries decreases with increasing strain (Figure 14) and correlates approximately with the size of α-platelet fragments formed *via* boundary splitting during deformation and/ or subsequent annealing. Ito *et al*.[125] also deduced that fragments which are slightly *smaller* than that expected based solely on the spacing of deformation-induced α/α boundaries were a result of additional α/α sub-boundaries formed *during* annealing. These latter boundaries evolve from platelet regions with sizeable (continuously-varying) lattice rotations but no high-angle boundaries. Other investigations have shown that the evolution of sub-boundary misorientation/spacing and thus boundary splitting is also dependent on the thickness of alpha lamellae/laths, temperature-dependent phase
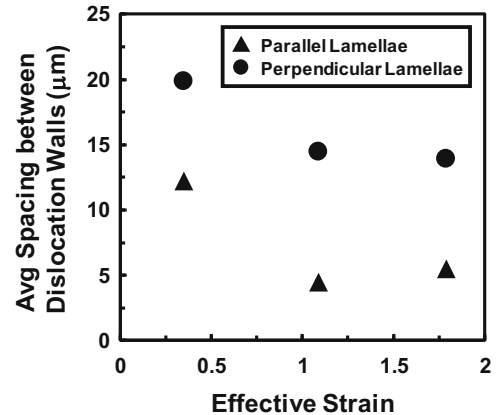

Fig. 14—Strain dependence of average spacing between dislocation walls/boundaries in Ti64 lamellae lying at an angle with respect to the compression axis of 0 to 45 deg ("parallel lamellae") or 45 to 90 deg ("perpendicular lamellae").[125]

fractions (which can lead to splitting of β layers during near-transus hot working), and strain rate and temperature which affect the recovery processes responsible for sub-boundary formation *per se*.[126–128] Such interactions warrant further research to develop a holistic understanding, however.

Despite its effect on the groove angle (δ) and slope (m) in the boundary splitting analysis (Eqs. [14a] and [14b]), the evolution of α/β interface energy with increasing strain has received little attention. The only notable investigation in this area appears to be that of Zherebtsov *et al*.[129] Their analysis indicated that the energy of a lamellar α/β interface in Ti64 is initially relative low (~0.05 J/m²), and increases during hot working to ~0.26 J/m² at a strain of ~0.8. A similar conclusion regarding the evolution of the α/β interface during straining can be inferred from measurements of the deterioration in the Burgers orientation relation (BOR) between the α and β phases in the lamellar structure during straining.[124,130] Such changes may be thought of as an indirect indicator of the degree of local deformation at/near the interface. During *warm* working of Ti64 and Ti-5Al-5-Mo-5V-1Cr-1Fe (the latter β alloy chosen due to the retention of a large amount β phase at room temperature), for example, deviations between the

corresponding close-packed planes/directions of ~10° were noted by strains of ~0.25 with complete loss of the BOR (>20° deviation) by a strain of ~0.5.[124,130] A similar result was found in research involving reversed torsion of Ti64 with a colony-α microstructure at 1088 K (815°C).[131] Here, the BOR was preserved during forward + reversed torsion when the imposed strain increment was less than the critical value required to initiate dynamic spheroidization, *i.e.*, 0.3 to 0.6.

2. Kinetics

The hot (and warm) deformation of α/β titanium alloys with a lamellar- or acicular-α microstructure leads to noticeable variations in strain from colony to colony as well as within a given colony. For this reason, measurements of the kinetics of dynamic spheroidization (in terms of fraction spheroidized as a function of strain) represent averages over the entire microstructure. Therefore, they provide broad engineering guidelines for design of manufacturing processes, but do not have a specific physical significance.

It is commonly observed that hot working leads to the kinking of α platelets (Figure 15).[34,35,132–134] The locally-higher strains in kinked regions and at prior-β-grain boundaries and colony boundaries bring about the initiation of dynamic spheroidization at modest macroscopic strains (~0.5). Moreover, EBSD techniques have been indispensable in elucidating the relationship between local crystallographic orientation, deformation heterogeneity, and spheroidization, *e.g.*, the work of Bieler and Semiatin.[135] Their assessment relied on the fact that the c-axis and one of the prism planes within an α lamella lay almost parallel to its broad face.[136] Thus, colonies for which the c-axis of the α phase lies close (<10°) to the compression direction are in a hard orientation (due to the high critical resolved shear stress for $\langle c+a \rangle$ slip systems) and thus undergo little straining and dynamic spheroidization (Figure 16). Those colonies for which the c-axis lies at an angle between 15° and 75° comprise softer orientations and experience the most strain. In addition, these latter orientations suffer deformation on both basal $\langle a \rangle$ and prism $\langle a \rangle$ slip systems, thereby leading to boundary splitting on orthogonal planes, a necessary condition to produce fragments of α rather than strips of α. Last, lamellar

plates whose c-axis lies *perpendicular* to the compression direction (either initially or as a result of the rotation during hot working) may undergo large strains as well, primarily by the activation of prism $\langle a \rangle$ slip alone, and therefore are difficult to fragment into equiaxed particles. In addition to these fundamental conclusions, Bieler and Semiatin[135] also recommended the use of multi-directional forging (at appropriate angles and levels of strain) to spheroidize colony-α microstructures more effectively.

Measurements of the fraction spheroidized X_{DS} as a function of strain ε have typically been based on a critical aspect ratio of the width to thickness of α platelets of 2:1.[34,35,38,122,137–139] Although spheroidization does not involve nucleation-and-growth phenomenon *per se*, data often exhibit a sigmodal behavior which is sometimes fit to an Avrami curve. Such curves consist of a critical strain to initiate dynamic spheroidization and then sequential regions of slow (initial), rapid (intermediate), and slow (final-stage) spheroidization rate $dX_{DS}/d\varepsilon$ (Figure 17). The spheroidization rate typically increases with (i)
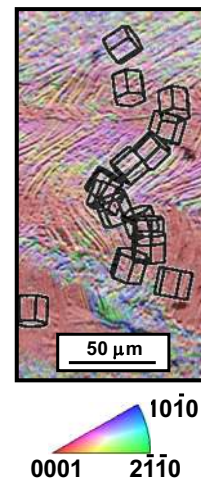

Fig. 16—EBSD compression-axis inverse-pole-figure map for a region in a Ti64 pancake forging illustrating the variation in dynamic spheroidization within and adjacent to hard-oriented (red) colonies. (Courtesy of T.R. Bieler.).
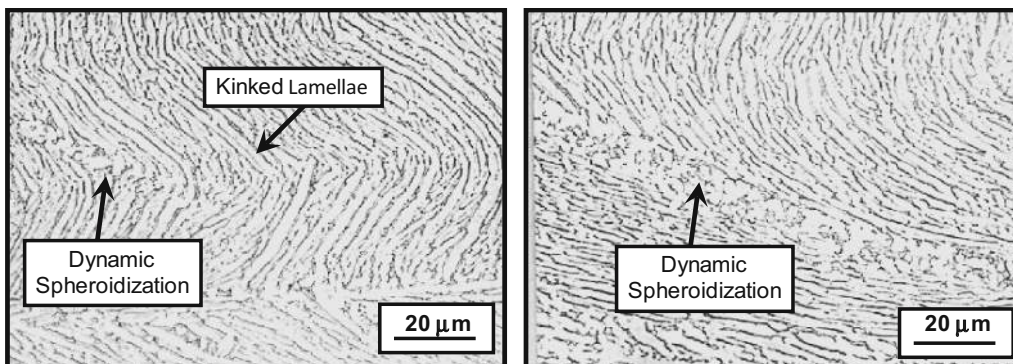

Fig. 15—Micrographs illustrating the kinking of α platelets and the early stages of dynamic spheroidization during hot compression of Ti64 at 1173 K (900 °C) and a strain rate of 0.001 s^{-1}.
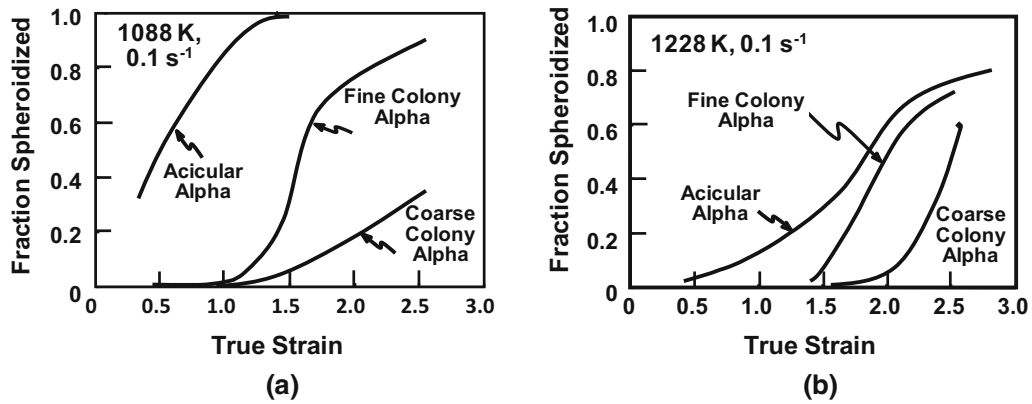
Fig. 17—Strain dependence of dynamically-spheroidized fraction in Ti64 with various starting microstructures deformed at 0.1 s^{-1} and temperatures of (a) 1088 K (815 °C) or (b) 1228 K (955 °C).[35]

increasing temperature and (ii) decreasing strain rate or initial α platelet thickness. Each of these trends can be rationalized on the basis of Eqs. [14a] and [14b] and the material parameters therein; the presence of pre-existing substructure may also accelerate dynamic spheroidization for the martensitic/acicular structure, especially at low temperatures In a similar vein, the size of dynamically spheroidized α particles tends to increase with increasing temperature and decreasing strain rate,[79,125,137] likely as a result of increasing spacing between the dislocation walls that underpin the boundary-splitting process. Some measurements[137] also reveal that *noticeably* larger alpha particles are developed during hot working when the strain rate is decreased specifically from 0.1 to 0.01 s^{-1}. This behavior may be influenced by concurrent spheroidization *and* dynamic coarsening and is worthy of further investigation.

3. Strain-path effect on dynamic spheroidization

Despite its industrial relevance, relatively little work has been performed to quantify the effect of strain-path changes during hot working on dynamic spheroidization of α/β (and β) titanium alloys with a lamellar starting microstructure. In the work of Korshunov et al.,[140] for instance, the effect of a variety of deformation modes (*e.g.* tension, torsion, reversed torsion) on the dynamic spherization of VT-9 was determined. Monotonic types of deformation (*e.g.* tension, torsion) produced noticeably more rapid rates of spheroidization than non-monotonic modes (*e.g.*, reversed torsion). In addition, sequential open-die forging along three orthogonal directions (so-called 'abc' forging) produced a microstructure which was only 25 pct. spheroidized after a total effective strain of 1.6.

Poths, Nicolaou, Muszka, and their coworkers[131,141,142] found a similar behavior during monotonic and reversed torsion testing of Ti64 with a colony-α microstructure at 1088 K (815°C). In the work of Poths et al.,[141] for example, the rate of dynamic spheroidization during reversed torsion was approximately *one-half* of that during monotonic ("forward") torsion (Figure 18). This behavior was explained on the basis of a reduced rate of α/α sub-boundary formation during reversed straining. In subsequent work,[131,142] the
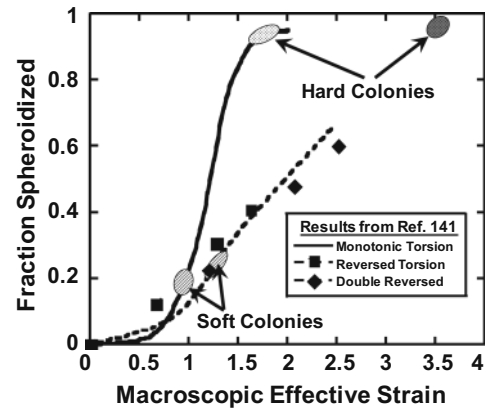

Fig. 18—Effect of strain path (monotonic torsion, reversed torsion, or doubly-reversed torsion) on dynamic spheroidization at 1088 K (815 °C) of Ti64 with a colony-α starting microstructure.[141] The ovals indicate the estimated macroscopic strains to spheroidize colonies with an initial soft or hard orientation.[142]

results of Poths et al.[141] were corroborated and extended. Specifically, Nicolaou and Semiatin[142] applied EBSD (in conjunction with a self-consistent model for strain partitioning[49]) to estimate the macroscopic strains required to spheroidize colonies with either "soft" or "hard" orientations. Not surprisingly, these results (also plotted in Figure 18) showed that soft colonies spheroidized early during straining and hard colonies at much higher strains. Nevertheless, when local rather than macroscopic strains were used to interpret the results, it was found that both soft and hard colonies required the same amount of deformation for dynamic spheroidization.

The torsion results of Muszka et al.[131] suggested that the level of strain at which deformation is reversed may also be important with regard to how work is stored and the concomitant rate of spheroidization. Specifically, for small strain increments (less than approximately 0.3), the microstructure was restored during the reverse portion of torsion. In such instances, less work is stored relative to that imparted during monotonic torsion to

the same total effective strain, and noticeable differences in dynamic *and* static spheroidiztion kinetics can be expected.

F. Static Spheroidization of α Lamellae

Due to the relatively-high strains required, full spheroidization of α/β titanium alloys with a colony- or acicular-α microstructure is usually not completed during hot working but rather statically during subsequent annealing. Two key mechanisms control the process, boundary splitting/fragmentation and termination migration.[108,143,144] As for its dynamic counterpart, boundary splitting during post-deformation annealing relies on residual stored work in the form of α/α (and in some instances β/β) sub-boundaries. Static morphological changes by this mechanism require relatively short times (of the order of 1 to 10 hours) before the process has been completed and/or the substructure itself has been reduced in effectiveness or eliminated during annealing. By contrast, the driving force for the second mechanism, termination migration, consists of the reduction in α/β interface energy by a classical spheroidization mechanism and usually transpires over much longer times, *i.e.*, 10 to 100 hours.

The analysis of boundary splitting during static heat treatment is identical to that embodied in Eqs. [14a] and [14b] with the proviso that the surface-energy and diffusivity terms likely change during annealing. A relatively-simple analysis of termination migration has also been developed and applied for α/β titanium alloys.[143,144] As for the elimination of lamellar branches described in Section III–D–2, the approach quantifies the diffusion of solutes from the edges of remnant lamellar fragments to the corresponding broad face(s) due to the concentration difference described *via* the Gibbs-Thompson equation. For the case of fragments in the form of thin circular pancakes, the normalized spheroidization time (τ_{vd}/τ') is given by the following relation:

$$\frac{\tau_{vd}}{\tau'} = \frac{\xi^3 - \left[0.328\xi^{7/3}\left(1 + \sqrt{1 - 0.763\xi^{-4/3}}\right)^2\right]}{4\left[\frac{2(1+\xi)}{3\left(0.5 - 0.572\xi^{-1/3}\right)} + \frac{0.5\xi^{1/3} + 0.665\xi^{2/3}}{3\left(0.143 + 0.934\xi^{-1/3}\right)}\right]} \quad [15a]$$

in which

$$\xi \equiv (w/d_\alpha) + 0.5 \quad [15b]$$

$$\tau' \equiv d_\alpha^3 R_g T / D_\beta C_F \gamma_{\alpha\beta} V_M \quad [15c]$$

Equation [15a] indicates a strong dependence of the spheroidization time on the initial fragment thickness (d_α) and the ratio of the initial diameter to thickness (w/d_α). Similar analyses of termination migration have also been performed for other α-fragment geometries such as thin, elliptical ones and rods.[145,146] The usefulness of the boundary-splitting and termination migration expressions to quantify static spheroidization has been validated for materials such as Ti64,[122,143] Ti6242,[145] and Ti-6Al-4Fe.[146]

Several recent investigations provide additional mechanistic insight and modeling refinements for static-spheroidization problems. Specifically, Roy and Suwas[147,148] performed a detailed investigation of static spheroidization of Ti64 which had been warm rolled prior to annealing, They documented important interactions between colony orientation, slip-system activity, non-uniform generation of sub-boundaries, and evolution of the α/β interface energy. In turn, these factors gave rise to noticeable non-uniformity in boundary-splitting behavior, which translated into variations in the shapes of fragments so produced and subsequent static spheroidization behavior *via* termination migration. The current picture of spheroidization by termination migration has also been enhanced by theoretical treatments using a phase-field modeling approach.[149] Details of the change in shape of pancake-shape α particles as they evolve into spheres have thus been described and contrasted with prior analytical results.[143,144] It was found that spheroidization can involve shape perturbations near the particle edges which were not taken into account in previous analytic approaches. The perturbations tend to retard the spheroidization process, thereby leading to predicted spheroidization times which are longer than those from treatments in which such effects were neglected.

Useful guidelines for industrial practice have also been gleaned from detailed measurements of the kinetics of static spheroidization for Ti64 and Ti6242.[145,150] For example, increasing the level of prestrain prior to annealing from ~0.5 to 1.5 leads to a decrease in the time to achieve a given spheroidized fraction by a factor of ~10 for Ti64 (Figure 19(a)). A prestrain dependence of spheroidization time was has also been found for Ti6242, but its magnitude is less[145] (Figure 20). However, a relatively short time for boundary splitting and long time for completion of termination migration has been noted for both Ti64 and Ti6242. Measurements of kinetics have also shown that the annealing temperature has a more important influence on static spheroidization than the precise hot-working temperature. For example, spheroidization kinetics for Ti64 at 1228 K (955 °C) were approximately an order of magnitude faster than those at 1173 K (900 °C), irrespective of whether the hot-work prestrain of 1.1 was imposed at 1173 K (900 °C) or 1228 K (955 °C) (Figure 19(b)).[150]

The retardation of dynamic spheroidization kinetics due to strain-path reversals during hot working, which was discussed in Section III–E–3, is also manifest during subsequent static annealing.[131] The trend is a result of the reduced number of sub-boundaries which are generated, a factor affecting both static and dynamic boundary splitting.

G. Coarsening of α Particles

A reduction in total α/β interface area/energy, which underlies termination migration, can also lead to noticeable coarsening of a dispersion of α particles subsequent to (or concurrent) with static spheroidization. For a
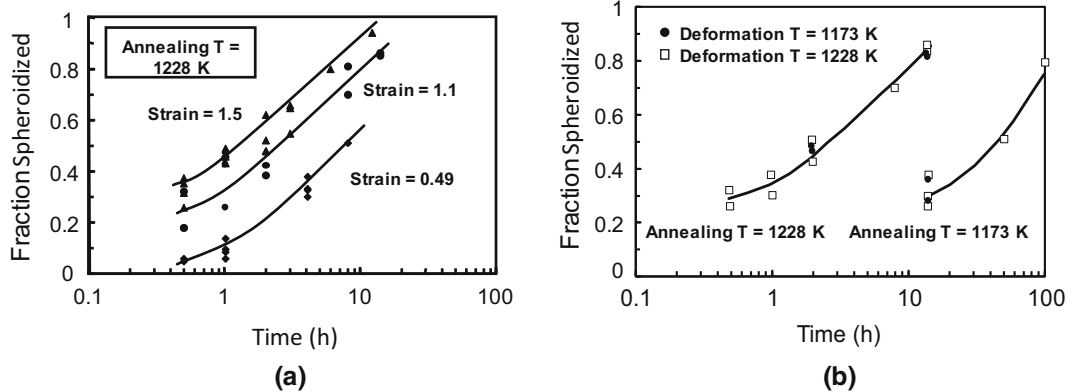
Fig. 19—Dependence of the kinetics of static spheroidization of Ti64 with an initial colony-α microstructure on: (a) Prestrain (at 1228 K, or 955 °C) or (b) deformation and annealing temperature (for a prestrain of 1.1)[150]
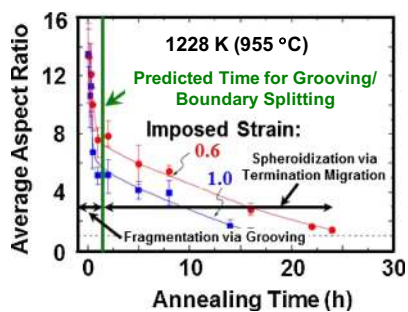

Fig. 20—Static spheroidization behavior in terms of the average aspect ratio of lamellae for Ti6242 samples with an initial colony-α microstructure that were prestrained and annealed at 1228 K (955 °C).[145] The results illustrate regimes of thermal grooving/ boundary splitting and spheroidization of the resulting fragments *via* termination migration.

wide range of temperatures, the static coarsening kinetics of α/β titanium alloys such as Ti64 and Ti6242[20,151–154] follow the LSW (Lifshitz, Slyosov, Wagner) formulation modified for a finite volume fraction of particles,[155] *i.e.*,

$$\bar{r}_\alpha^3 - \bar{r}_{\alpha o}^3 = K_{MLSW}(t - t_O) \qquad [16a]$$

in which $\bar{r}_\alpha$ and $\bar{r}_{\alpha o}$ denote the average radius at time t and $t_o = 0$, respectively, and K_{MLSW} is the coarsening rate constant.

$$K_{MLSW} = \frac{8g(\phi)D\gamma_{\alpha\beta}C_\beta(1 - C_\beta)V_M}{9RT(C_\alpha - C_\beta)^2[1 + \partial lnr/\partial lnC_\beta]} \qquad [16b]$$

In Eq. [16b], $g(\phi)$ describes the functional dependence of the coarsening rate on the volume fraction of particles (ϕ), and the other terms are the same as defined above. It has been found that the modified LSW formalism breaks down, however, for Ti64 at very low temperatures (T ~ 823 K (550 °C)),[156] presumably because of the very high proportion of α phase whose percolation through the β matrix interferes with the bulk diffusion of solutes assumed in the model formulation.

Expressions identical to Eqs. [16a] and [16b] also apply for α-particle coarsening that occurs during superplastic deformation.[152–154,157] In such instances, however, the value of D is higher by a factor of ~10 relative to that for static coarsening, likely because of the kinetic enhancement (pipe diffusion) associated with dislocation generation in the β matrix.

H. *Evolution of Crystallographic Texture*

Texture has a strong effect on final mechanical properties. Hence, extensive work has been performed to both measure and model texture evolution. A number of these efforts have been summarized in References 158 through 161, and thus will only be discussed here briefly.

Noticeable *deformation textures* in α/β titanium alloys can be developed during mechanical processing in either the β or α/β field. Because of its lower crystal symmetry, texture components in the α phase are usually stronger. The type and strength of the components, however, is dependent on deformation mode (*e.g.*, extrusion, rolling, upset forging, *etc.*) and processing temperature. For example, hot working of Ti64 ingots in the β field *via* upsetting followed by cogging (also known as "drawing" or "drawing out" in industrial parlance) gives rise to a ⟨110⟩ fiber texture in the β phase.[162] Large deformation *via* plate rolling in the β field gives to a marked "rotated cube" ((001)⟨110⟩) β-phase texture.[12] Hot working *via* plate rolling in the α/β phase field usually produces moderate-to-strong α-phase textures whose components often comprise basal poles parallel to the plate normal or the long-transverse direction. Various crystal-plasticity methods have been applied to predict deformation textures. These include, isostrain (Taylor), viscoplastic self-consistent, and crystal-plasticity-FEM analyses.[12,14,55,160,162–164] Typically, predictions mirror observed texture components, but simulated intensities tend to be stronger than those measured.

Extensive work has also been done to understand the development of the texture of the lamellar/acicular α phase formed by the decomposition of the high-temperature β phase during the cooling of α/β titanium alloys. Investigations of such *transformation* textures have dealt

with the formation of a subset of the twelve possible α-phase variants that may form in a given β grain (*i.e.*, variant selection) following annealing or hot working in the β or α/β phase fields. For the case involving processing in the β field, cooling rate, β grain size, and level of hot work have been proposed as variables affecting the degree of variant selection.[12,165–171] Rules to explain such phenomena include those based on (i) the most-highly activated slip system(s), (ii) a critical level of slip, or (iii) the preferential nucleation of variants at β grain boundaries for which there are nearly parallel $\{110\}_\beta$ planes in the two adjacent grains thus leading to nearly parallel $[0001]_\alpha$ directions in the variants on either side of the boundary. Other rules based on the minimization of local elastic strain energy associated with the transformation and/or some form of cooperative transformation between the variants formed in a grain and its nearest neighbors have also been proposed.[104,172,173] Furthermore, there is evidence for an influence of neighboring β grains on variant selection. This includes observations of a so-called "memory effect"; *i.e.*, the re-appearance of specific variants within each grain during repeated heating and cooling cycles above and below T_β.[173,174]

The transformation texture of secondary-α plates formed within matrix β grains during cooldown following deformation or heat treatment in the α/β field has also been documented. For instance, observations of alpha variants whose orientations are similar to those of the primary alpha[175,176] have been rationalized on the basis of stresses developed during cooling due to differences in the coefficients of thermal expansion of the two phases. Such biasing of the texture of the secondary α by that of the primary α has been quantified using a minimum strain-energy criterion which was successful in predicting observed textures.[177] Alternatively, it has been postulated that the anisotropic thermal contraction of primary α during cooling may activate slip on selected $\{110\}$ planes in the β phase that leads to biasing the formation of secondary-α variants.[178]

I. *Future Research Opportunities*

Despite extensive research in the area of microstructure evolution for α/β titanium alloys, a plethora of issues and research opportunities remain. These include the following

- Substructure evolution in the β phase: The effect of substitutional solutes on the kinetics of the formation of subgrains/grains in the β phase during hot working in the β or α/β phase fields should be quantified.
- Substructure evolution in the α phase: A fundamental understanding of substructure evolution in single-phase and colony α is critical for the development of advanced physics-based models for deformation (and transformation) texture evolution, dynamic and static spheroidization, *etc*. Issues such as the relation between imposed deformation, the evolution of geometrically-necessary dislocations vs

statistically-stored dislocations, and the size/spacing/misorientation of subgrains or dislocation walls (in equiaxed vs lamellar microstructures) could provide useful insights necessary for physics-based models. This work should also seek to quantify the three-dimensional (3D) nature of substructure evolution and its dependence on local crystallographic orientation and slip-system activity. In this regard, 3D serial sectioning using a focused-ion-beam (FIB) coupled with EBSD and/or electron-channeling-contrast imaging (ECCI) could be quite useful especially for α/β titanium alloys with a colony-α microstructure.

- Effect of α/β hot working variables on subsequent recrystallization in the β phase field: With advent of high-speed EBSD techniques, additional insight could be gained on the effects of level of α/β deformation, hot working temperature/phase fractions, *etc*. on substructure evolution in a lamellar microstructure which controls subsequent recrystallization in the β field. For example, spatial variations in substructure which may give rise to uniform or non-uniform recrystallization (and grain growth) could be identified.
- Grain-boundary energy and mobility measurements for the β phase: To simulate texture-controlled grain growth in the single-phase β field, detailed measurements of grain-boundary properties for alloys such as Ti64 (as well as β titanium alloys) are needed. Such data would also be useful for the calibration/validation of first-principles models for such properties.
- Coarsening of α lamellae during extended heat treatment in the α/β field: Because of its importance with respect to dynamic and static spheroidization, the three-dimensional nature of platelet geometry and coarsening behavior should be documented and modeled. This work could make use of modern (automated) serial-sectioning techniques, synchrotron observations, *etc*.
- Strain-path effects on dynamic and static spheroidization and plastic flow: Industrial TMP practices often include strain-path changes, but only limited work has been performed in this area. Thus, R&D would be useful to establish path effects on plastic flow and microstructure/substructure/texture formation, especially for the breakdown of the colony-α microstructure. This work may uncover strain paths that reduce the number of hot-working steps, produce more uniform microstructures, and/or eliminate or reduce defects such as those described in Section IV below.
- Texture modeling: Accurate *quantitative* texture models would provide a critical design tool to manufacture titanium parts with desirable location-specific properties. However, a number of areas likely require additional research to make this a reality. These include (i) Development of high-fidelity, user-friendly texture-modeling codes, (ii) formulation of high-temperature constitutive relations that describe pertinent slip, recovery, strain-hardening, *etc*. processes for equiaxed, lamellar, and "intermediate" microstructures, with due

regard for appropriate length scales, and (ii) validation of *quantitative* rules for α-variant selection as a function local crystallographic neighborhood, cooling rate, and stored work, the latter provided by a deformation-texture code.

- Dynamic transformation of α/β titanium alloys: Beginning in the year 2000, a number of investigations have presented both experimental evidence and theoretical (thermodynamic) justification for a *dynamic* reduction in the volume fraction of α phase relative to that based on equilibrium (no-deformation) conditions. The observations have covered a range of strain rates (including superplastic and non-superplastic), types of deformation (monotonic vs multistage with interpass dwells), and starting microstructures (equiaxed vs colony α).[179–182] Dynamic transformation in titanium alloys deserves additional attention both as a fundamental phenomenon and with regard to its effect on industrial processing. For example, quantitative in-situ (synchrotron) studies may help to clarify the kinetics of such transformations.

- Epitaxial recrystallization: Recently, it has been shown that a process known as epitaxial recrystallization may also lead to equiaxed α and β during the hot working of an acicular starting structure for the metastable β titanium alloy Ti-5Al-5Mo-5V-3Cr.[183] This mechanism comprises nucleation (and subsequent growth) of new strain-free β (or α) grains at incoherent α/β interfaces, and results in lower-energy, partially-coherent interfaces and restoration of the BOR between α and β. The latter can have a substantial effect on the nature of slip transfer during subsequent processing or service. . Moreover, the occurrence of epitaxial recrystallization may lead to the generation of special β grain boundaries which can affect the selection of grain-boundary-alpha variants. Research on other β and α/β titanium alloys to establish the generality of this mechanism and the processing conditions under which it occurs would be useful.

IV. DEFECTS

The TMP of α/β titanium alloys may lead to a variety of undesirable defects whose size spans the length scale from nanometers to multiple millimeters and which can be deleterious to service properties, especially fatigue crack initiation and growth. Such anomalies may have a source which is microstructural or gross metal flow in nature, or both. At the low end of the spectrum, hot (and warm) working may give rise to voids with sizes between 100 nm and 50 μm. In industrial practice, such cavities are usually referred to as "strain-induced porosity" or SIP. Although most commonly developed during α/β hot working of the colony-α microstructure, cavities may also be formed during β-field deformation of coarse-grain, beta-rich α/β titanium alloys. Having sizes of the order of 100s to 1000s of microns, microtextured regions (MTRs), also known as macrozones, consist of areas of partially (or even fully) spheroidized alpha particles with the same or nearly the same crystallographic orientation. MTRs can be retained after hot-working operations designed to convert a colony-α microstructure to an equiaxed one. Undesirably-coarse or abnormal β grains with sizes of several to many millimeters may be developed during processes comprising α/β forging and final β annealing, which are often used to impart a transformed structure for fracture-critical/damage-tolerant structural components. The current state of understanding related to the occurrence of SIP, MTRs, and coarse/abnormal β grain growth is summarized in the subsections below.

Gross metal-flow defects are usually related to material constitutive behavior, die design, processing conditions, or a combination of all three.[184] The tendency to form macroscopic shear bands during conventional hot forging, for example, is exacerbated by high degrees of material flow softening/low strain rate sensitivities, plane-strain deformation, and processing conditions which lead to high thermal gradients or low temperatures within the workpiece during forging. The latter includes the use of preforms with thin cross sections, slow forging speeds, and low preheat temperatures. Two characteristics which make α/β titanium alloys especially prone to shear-band formation include their large dependence of flow stress on temperature and, for preforms with a colony-α preform microstructure, high flow softening rate. Improper choice of preform/die design, lubrication, or process variables can also give rise to other flaws in α/β titanium forgings such as laps, folds, surface cracks, and flow-through defects.[184]

A. Cavitation and Fracture

The nature of cavity formation (*i.e.*, cavitation) and fracture during hot working of α/β titanium alloys has been quantified using both phenomenological and mechanistic approaches. Early work focused on gross fracture during hot tension testing and determination of the reduction in area as a function of strain rate and temperature. For example, it was shown that a variety of near-α and α/β titanium alloys with a colony-α microstructure exhibit high ductility at temperatures near T_β, but a noticeable drop at temperatures of the order of $T_\beta - 50$ K ($T_\beta - 50$ °C) and lower.[185–188] This behavior was explained qualitatively on the basis of intergranular failures initiated within the soft layer of β lying between the harder grain-boundary α and colony-α sideplates or as a result of slip incompatibility between the sideplates and the grain-boundary α.

Subsequent investigations verified that cavity initiation during the bulk hot working of α/β titanium alloys with a colony-α microstructure does indeed occur at the prior-β grain boundaries as well as interfaces between adjacent colonies within the same grain (Figure 21).[189,190] Furthermore, examination of forgings with free-surface cracks or internal cavities indicated that such damage was associated with the generation of secondary tensile stresses. It was determined that the initiation of observable cavities (using a "standard" optical magnification of 500X) could be
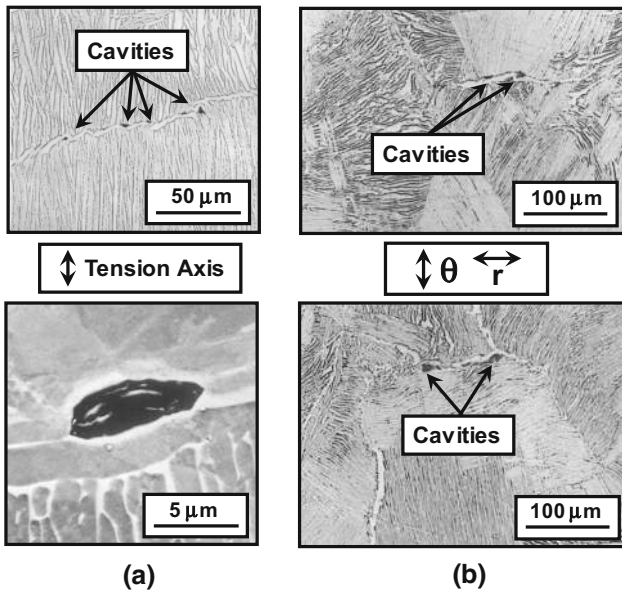
Fig. 21—Optical micrographs illustrating the nucleation of cavities in Ti64 samples with an initial colony-α microstructure that were deformed at 1088 K (815 °C) via (a) uniaxial tension[189] or (b) pancake forging.[190]

correlated to uniaxial tension observations using the Cockcroft-and-Latham (C + L) maximum-tensile-work criterion[190–193] developed originally to explain the occurrence of gross fracture under arbitrary stress states:

$$C_{i,f}^* = \int_0^{\bar{\varepsilon}_{i,f}} (\sigma_t/\bar{\sigma}) d\bar{\varepsilon} \qquad [17]$$

In Eq. [17], C_i^* and C_f^* denote the critical damage parameter for cavity initiation or fracture, respectively, usually determined from a tension test. The integral on the right-hand side is the work done by maximum tensile stress for an arbitrary stress/strain path (σ_t), normalized by the effective stress ($\bar{\sigma}$), through the effective strain ($\bar{\varepsilon}$). For a tension test in which necking is absent or minimal, C_i^* and C_f^* are thus equal to the effective strain at which cavities nucleate (typically determined by metallographic sections) or fracture occurs, respectively. The engineering efficacy of this approach has been demonstrated for the prediction of cavity initiation and gross fracture in simple (pancake) and complex forgings of Ti64, e.g., Figure 22.[190] In addition, maps illustrating the temperature and strain rate dependence of C_i^* have been developed for Ti64 with a preform structure of colony-α or a corresponding, partially-spheroidized condition.[193]

The micro-mechanisms of cavity nucleation and growth during subtransus hot working have also been investigated, largely for Ti64 with a colony-α microstructure. Based on observations of thin, elongated ("penny-shaped") cavities during early stages of cavitation (Figure 21), Ghosh et al.[194,195] formulated a constrained-plasticity model to describe nucleation. As initially implied by the work of Suzuki et al.,[185–187] the
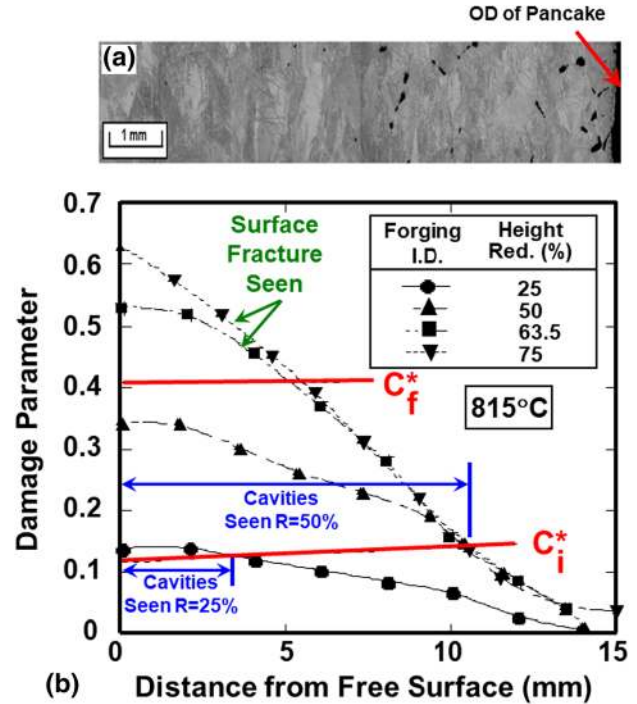

Fig. 22—Observations and model predictions for cavities formed in pancake forgings of Ti64 with an initial colony-α microstructure: (a) Macrograph on the mid-thickness (equatorial) plane of a pancake forged to a 50-pct. height reduction at 1173 K (900 °C) and (b) comparison of FEM calculations of the radial variation of the C + L damage parameter for various height reductions (black lines, data points), critical damage factors C_i^* and C_f^* from tension tests (red lines), and observations of cavity depths (indicated in blue) and surface fracture (green) in samples forged at 1088 K (815 °C).[190]

growth of slip-intersection-generated nanovoids, located in the soft layer of β between harder regions of grain-boundary α and colony α, formed the basis of the model. By this means, the effect of material properties (flow stress, strain-rate sensitivity as a function of temperature) on the expansion of penny-shaped cracks was quantified.

Once cavities have grown to a size several times that of a characteristic dimension of the microstructure (e.g., the thickness of the β layer adjacent to the grain-boundary α), further enlargement is often assumed to be controlled by a more isotropic state of plasticity. Under uniaxial-tension conditions, the growth of an isolated spherical void of radius r as a function of strain ε is then described using the relation[196,197]:

$$dr/d\varepsilon = \eta r/3 \qquad [18a]$$

$$\text{or} \quad r = r_o \exp[(\eta/3)(\varepsilon - \varepsilon_o)] \qquad [18b]$$

in which η is the cavity-growth parameter (equal approximately to the inverse of strain-rate sensitivity of the flow stress), and r_o is the radius of a cavity at a strain of ε_o when it first becomes stable. The measurement of the growth rate of individual cavities and thus the value of η is confounded by concurrent cavity nucleation and coalescence. To remedy this problem, the overall cavity volume fraction C_v is measured, and

its dependence on strain is fit to a relationship similar to Eqs. [18a] and [18b],[197] *viz.*:

$$C_V = C_{V_O} \exp(\eta_{APP}(\varepsilon - \varepsilon_O)) \quad [19]$$

The apparent cavity growth rate η_{APP} and the fitting parameter C_{V_O} are determined from semilog plots of measurements of C_v vs ε. A series of parametric simulations have led to relations between η_{APP} and η.[197]

The description of plasticity-controlled cavity growth as described in Eqs. [18a] and [18b] and [19] requires several modifications for the application to forging under complex stress states, in general, and to plastically-anisotropic materials such as α/β titanium alloys, in particular. The first of these comprises relating the uniaxial cavity-growth parameter η to that pertinent to complex states of stress in metalworking operations such as forging, η^{ts}; typically η^{ts}/η is linearly related to the ratio of the mean-to-effective stress, *i.e.*, the stress triaxiality. Second, the occurrence of cavitation in alloys such as Ti64 with a colony-α microstructure has been found to depend on the macroscopic *and* local states of stress and strain. In particular, cavity growth is most noticeable at interfaces between adjacent hard and soft colonies[198–200] (Figure 23). To predict the size of cavities in such situations, Nicolaou *et al.*[201] developed a mesoscale model to quantify the local stress triaxiality (and thus η^{ts}) and the strain partitioning between colonies with larger and smaller Taylor factors (M_h, M_s). The analysis made use of stress-equilibrium/yield-function equations and the self-consistent model described in Section II–C. Employing nucleation strains

Fig. 23—EBSD inverse-pole-figure maps for Ti64 samples (with an initial colony-α microstructure) in which cavities developed during hot deformation at 1088 K (815 °C) *via* (*a*) uniaxial tension,[198] (*b*) pancake forging,[199] and (*c*) torsion testing.[200] The superimposed hexagons indicate the orientations of (hard and soft) colonies adjacent to some of the cavities.

measured in notched tension tests (with various degrees of stress triaxiality), the size of the *largest* cavities in pancake forgings as a function of M_h/M_s were thus predicted successfully (Figure 24).[200,201]

Strain path can also play an important role in cavitation during hot working of α/β titanium alloys. For example, during hot torsion of Ti64 with a colony-α microstructure, it was found that cavities generated during forward straining shrink during reversed straining but at a slower rate than during prior growth.[202] Such observations have been explained in the context of changes in the sign and magnitude of the stress triaxiality in regions in which cavities first form between hard and soft colonies. Specifically, local triaxiality changes are associated with the reversal of straining *per se* as well as a decrease in flow softening rates at high strains. The beneficial effect of a change in strain path has also been observed in deformations comprising torsion followed by uniaxial compression.[203] In such cases, the shrinkage rate is faster than in reversed torsion due to the higher level of (compressive) stress triaxiality. However, in both reversed torsion and torsion followed by compression, the rate of cavity closure decreases with increasing strain, thus indicating that very large deformations may be required to fully close pores. In related work, the beneficial effect of compressive stress triaxiality on cavity closure was quantified using FEM analysis.[204] This effort also elucidated the effect of cavity shape and initial orientation on closure behavior.

Unfortunately, there appears to be no reports of whether cavity closure correlates with cavity sealing, *i.e.*, the formation of a metallurgical bond across the interfaces brought into intimate contact with each other. The pressure-temperature-time combinations that may be needed in such cases can perhaps be estimated from classical models of diffusion bonding.[205]

B. *Microtexture Regions (MTRs)*

Originally documented in the 1990s using EBSD,[206] MTRs in near-α and α/β titanium alloys (Figure 25[207,208]) seriously detract from service properties such as cold-dwell fatigue resistance.[209,210] However, only a relatively-modest amount of effort has been expended to document their source and techniques to alleviate the condition.

All of the α in a specific colony, which is newly formed during cooling following processing in the β field, has the same orientation. Hence, in a formal sense, it may be said that MTRs exist *prior* to α/β hot working. Moreover, in some instances, large crystal rotations leading to noticeable *macrotextures* may result in MTRs whose extent may comprise 2 or more colonies.[211]

The elimination MTRs comprises a combination of spheroidization and rotation of individual α particles. Several factors make this difficult to accomplish for every colony in an aggregate. As discussed in Section III–E–2, the first is related to the fact that colonies with soft- and hard- orientations relative to the imposed deformation undergo a greater or lesser amount of strain, respectively[135]; therefore, MTRs tend to
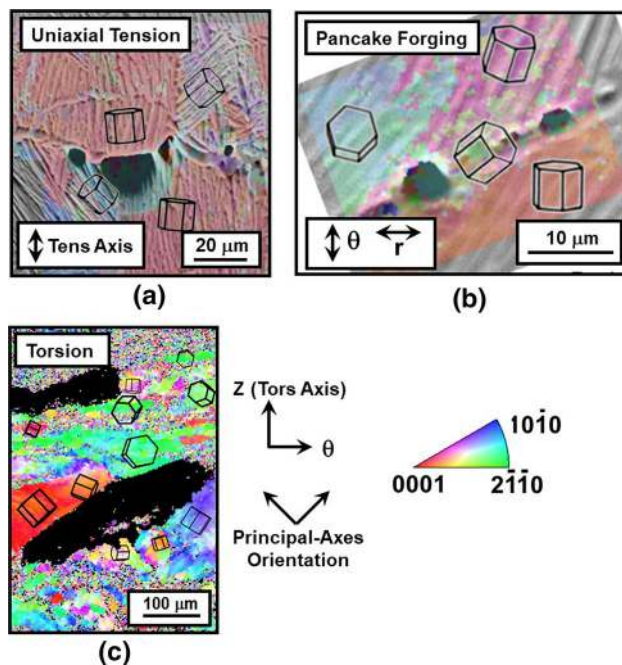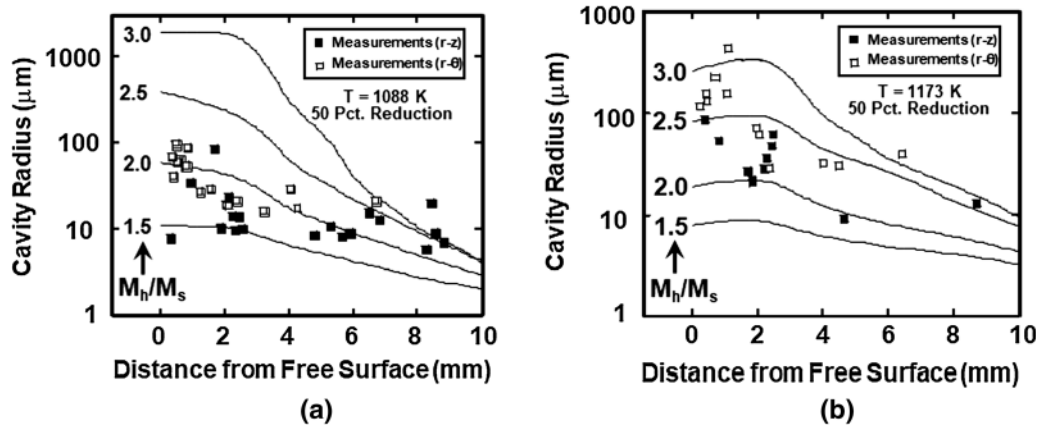
Fig. 24—Comparison of measurements and model predictions of the dependence on the Taylor-factor ratio (M_h/M_s) of the size of the largest cavities developed in Ti64 with an initial colony-α microstructure during hot pancake forging to a 50-pct. height reduction at (*a*) 1088 K (815 °C) or (*b*) 1173 K (900 °C).[201]
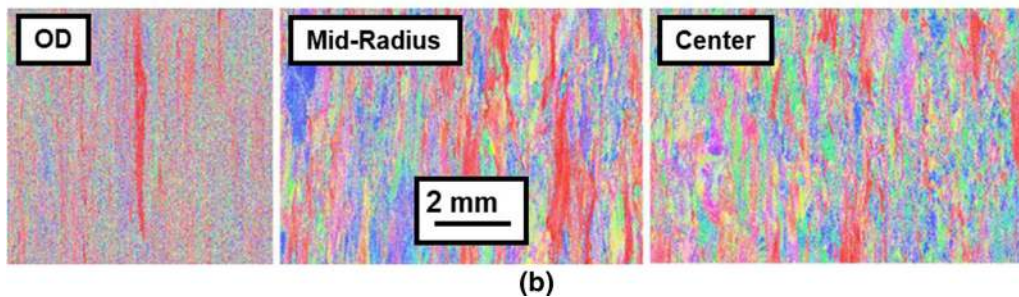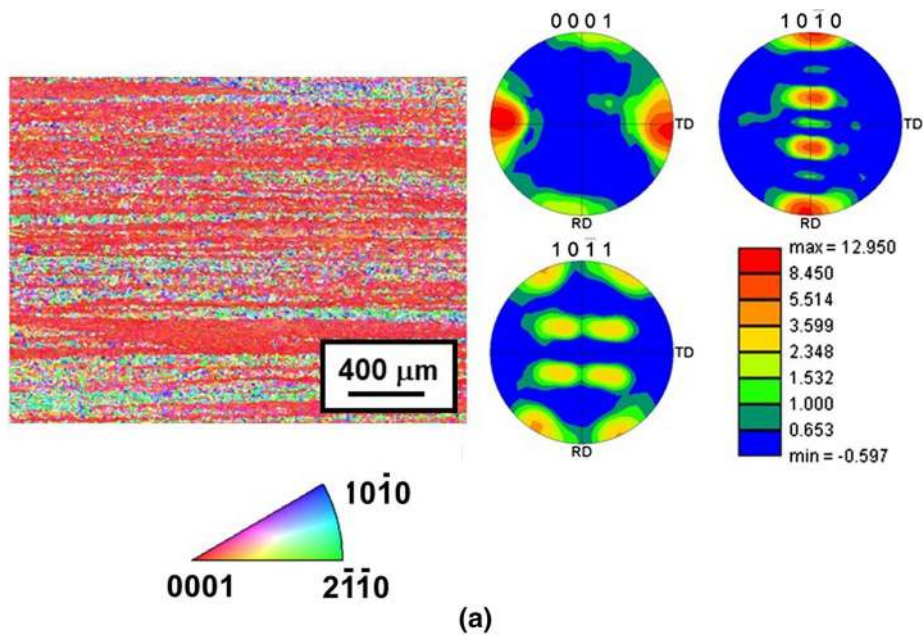

Fig. 25—EBSD data illustrating microtexture regions in wrought α/β titanium mill products: (*a*) 32-mm-thick hot-rolled plate of Ti64 (transverse-direction inverse-pole-figure map and corresponding pole figures)[207] and (*b*) 209-mm-diameter Ti6242 billet (radial-direction inverse-pole-figure maps at various radial locations).[208]

correlate with initially-harder colonies. Second, although the formation of subboundaries within α lamellae can give rise to large ("tilt-like") misorientaions between adjacent material elements, such a process must

occur in two orthogonal directions, generally necessitating the activation of both prism $\langle a \rangle$ and basal $\langle a \rangle$ slip (or pyramidal $\langle c+a \rangle$ slip).[135,147] This is most readily accomplished for colonies whose c-axes lie at an oblique

angle to the principal axes of deformation. For colonies with other orientations, a change in strain path prior to the development of soft, *locally*-spheroidized regions is necessary. The presence of such soft regions would increase the difference in flow stress between them and remnant unspheroidized material whose relative flow stress is now even greater as a result of both its crystallographic orientation *and* lamellar morphology. Last, the overall amount of rotation that can be accommodated by the individual lamellae within a given colony is limited by the requirement of compatibility with surrounding colonies. Adjacent lamellae thus tend to rotate relative to each other, and these rotations tend to be compensatory in nature.[124] It has also been found that static spheroidization (following hot working) does not introduce a large number of new orientations and thus cannot be used to lessen the severity of MTR formation.[211]

The severity of MTRs associated with spheroidized primary-α particles (and the detriment to mechanical properties) can be further exacerbated by the tendency of secondary-α platelets *with a similar orientation* to form in the β matrix during cooling.[176,212,213] However, it has been suggested that such an effect can be reduced for β grains for which the BOR with surrounding primary-α particles has been totally eliminated or by imposing a high cooling rate following final α/β heat treatment in order to develop multiple variants within each β grain.[214]

Fundamental investigations of MTR evolution have been complemented by laboratory and industrial-scale process-development efforts to eliminate the defect. Perhaps the first of these consisted of the pioneering work of Salishchev and his colleagues at the Institute for Metals Superplasticity Problems (and then at Belgorod State University) in Russia. In the early 1990s, for example, they developed various techniques involving isothermal α/β warm working of billets having an initial transformed microstructure to produce a uniform, fine-grain microstructure without MTRs.[215] In particular, the transformed structure was first spheroidized by applying a moderate-to-high strain (at a strain rate of 10^{-3} s^{-1}); a fine α-particle size was thus developed. Further imposed deformation then occurred superplastically, resulting in interface sliding and randomization of the orientations of individual α particles. Various processing alternatives, including multistep processing at successively lower temperatures and multi-axial forging, were also introduced.[216,217]

A number of other techniques for reducing/elimination MTRs can also be found in the patent and scientific literature. Patents include one based on a two-step process consisting of (i) a high, subtransus-temperature heat treatment followed by water quenching to produce multiple variants of secondary-α platelets within each β grain, thereby disrupting the continuity of the orientations of primary-α particles in each MTR and (ii) a second heat treatment step at a lower temperature to coarsen the secondary-α produced in the first step.[218] Other patents are based on multi-step hot working at successively lower temperatures in the α/β phase field, each with an intermediate cooling stage.[219,220]

Presumably, such processes introduce secondary-α (following each hot-working-and-cooling stage), which is subsequently spheroidized or rotated in the subsequent processing stage(s). In a similar vein, a process comprising α/β hot working of billets/preforms which have been β annealed and water quenched to produce a basketweave-α microstructure (*i.e.*, multiple variants at any given location) has been proposed.[221] It may be surmised that this latter method might be restricted to section sizes for which the basketweave-α microstructure can be developed during the quench operation, however.

In the scientific literature, Gey *et al.*,[214] demonstrated that a change in strain path involving redundant work can be beneficial in eliminating MTRs in Ti834 forgings. In their effort, α/β close-die *forging* (to strains of the order of unity) along a direction *parallel* to the *extension* (billet) axis during primary fabrication *via* cogging was very beneficial. The efficacy of such a strain-path change (elongation then compression) was also mirrored recently in crystal-plasticity FEM simulations for Ti6242.[222] These simulations also indicated that compression *perpendicular* to the axis of billet with a $\langle 10\bar{1}0 \rangle$ fiber texture can lead to a beneficial amount of "smearing" of the orientations of the α particles in an MTR whose c-axes were aligned originally with the compression direction.

C. *Coarse/Abnormal β Grains*

As suggested by Figure 9,[88] the early stages of microstructure evolution during β annealing following α/β hot working has been observed to be controlled by (i) the dissolution of primary-α particles (which pin β grain boundaries) and (ii) the subsequent growth of a group of β grains which are highly-misoriented relative to a matrix of β subgrains. At longer times, the growth of the highly-misoriented grains is limited by impingement. Hence, the propensity for the formation of regions of coarse β grains (or a few grossly-abnormal, or rogue, grains) is likely controlled by the number density of highly-misoriented grains present during the early stages of annealing.

Prior to impingement, the rate of growth of a grain of radius R (having a mobility M and boundary energy γ) is given by the following relation[88,223]:

$$\frac{dR}{dt} = M\left(\frac{\bar{\gamma}}{\bar{R}} - \frac{\gamma}{R}\right) \qquad [20]$$

in which $\bar{\gamma}$ and $\bar{R}$ denote the average boundary energy and radius of the subgrains. Thus, a collection of small subgrains (*i.e.*, a β microtexture) with misorientations of ~5 to 10 deg and a small enough size relative to that of the highly-misoriented grains (such that $\bar{\gamma}/\bar{R} > \gamma/R$) can provide a large driving force for the growth of the latter. Such subgrain misorientations would possess a *moderate* subboundary energy (relative to that of a high-angle boundary), but exhibit limited subgrain growth due to low boundary mobility.

Several recent efforts have shed light on the processing conditions that give rise to the deleterious β microtexture and thus the tendency for the formation

of the coarse-grain condition in Ti64. Pilchak et al.,[88] for example, showed that plane-strain (subtransus) sheet rolling tends to produce a strong rotated-cube deformation texture which is strengthened considerably during the early stages of β annealing due to orientation-dependent nucleation and growth.[224] The average misorientation between the β subgrains in this work was ~6°.

In a subsequent modeling effort,[225] the sharp rotated-cube texture developed in plane-strain was reproduced using viscoplastic, self-consistent (VPSC) crystal-plasticity calculations. These results also indicated that the phase fractions present during hot working (and thus strain partitioning between the phases) has a noticeable effect on the sharpness of the rotated-cube component. For an imposed strain of ~1.2, the predicted texture was very strong when the primary-α fraction was ~0.25 (typical of a conventional hot-working temperature), but was considerably weaker for lower-temperature processing at which the fraction was 0.50 (Figure 26). The latter behavior can be rationalized based on the fact that more of the imposed strain is accommodated by the α phase at lower temperature, thus retarding/mitigating the formation of a β microtexture. The usefulness of the VPSC-model results has been established using the sidepressing of cylindrical preforms measuring 63-mm diameter x 190-mm length. For this metalworking operation, a state of nominal plane strain is realized at the midlength. Compression to a true thickness strain of ~1.0 or 0.5 at $T_\beta - 40$ K ($T_\beta - 40$ °C), at which the α fraction is ~0.25, did or did not lead to a coarse-grain condition, respectively, during subsequent β annealing (Figures 27(a), (b)). These observations suggest that a critical deformation of ~1 in a plane-strain mode can trigger the formation of coarse grains. By contrast, sidepressing to a strain of ~1.0 at $T_\beta - 100$ K ($T_\beta - 100$ °C), at which the α fraction is ~0.50, did not result in a grain-size anomaly during β annealing (Figure 27(c)). This observation can also be rationalized on the basis of the VPSC calculations.

Other deformation modes have also been found to predispose α/β titanium alloys to the formation of coarse-grain regions during subsequent β annealing. These include the cogging ("drawing out") of square billets, in which a cube texture can be developed in the β phase and result in a coarse-grain condition during β annealing.[226]

Modeling the evolution of grain-size anomalies during heat treatment in the β field has been accomplished both analytically (e.g., based on Eq. [20][88]) and numerically

Fig. 27—Macrographs of transverse sections of sidepressed Ti64 cylindrical preforms which were β annealed at 1311 K (1038 °C) for 1 hour following subtransus forging at (a, b) 1228 K (955 °C) or (c) 1186 K (913 °C) to a reduction of (a) ~40 pct. or (b, c) ~65 pct.
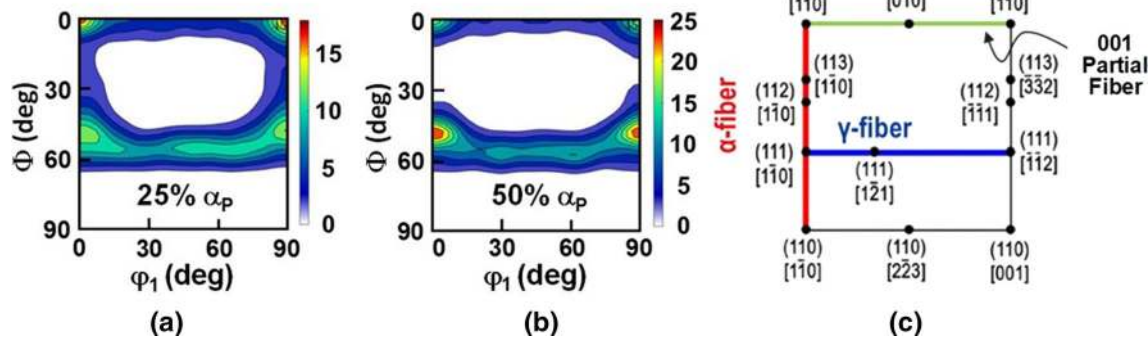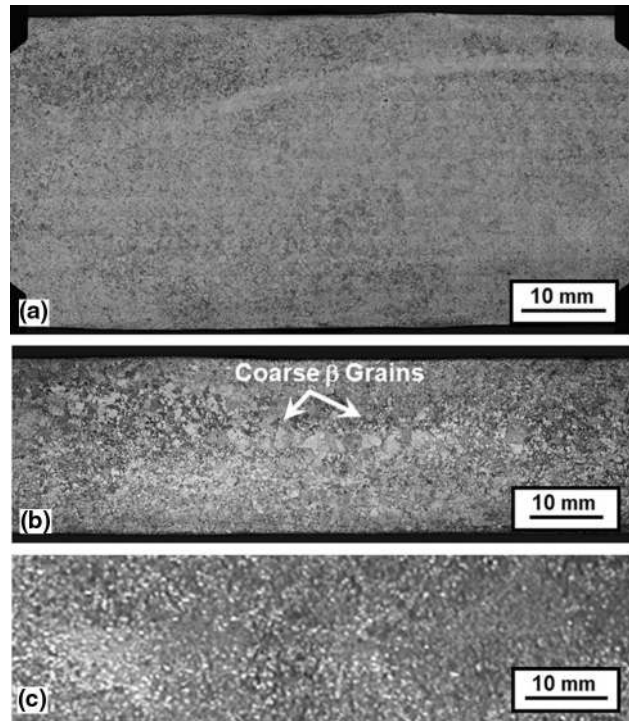

Fig. 26—VPSC simulation predictions of the orientation distribution function (φ_2 = 45 deg section) showing the intensity of the rotated-cube texture component for a 65-pct. reduction ($\varepsilon \sim 1$) of Ti64 in a plane-strain-compression mode for a microstructure comprising (a) 25-pct. α (T ~1228 K, or 955 °C) or (b) 50-pct. α (T ~ 1173 K, or 900 °C).[225] For reference, the ideal deformation-texture components typically observed in bcc crystals are shown in (c).

(using Monte-Carlo (MC) simulations[227,228]). Using the latter method, the effect of texture intensity/breadth (*e.g.*, the fraction of high-misorientation grains) on the tendency for abnormal-like growth has been determined and summarized in the form of processing maps.[226,227]

D. *Future Research Opportunities*

Further research into the evolution of defects and methods to avoid them is needed to provide well-validated tools to manufacturing-process and system designers. Areas that warrant attention include the following:

- Cavity initiation: The development and validation of quantitative descriptions of the mechanism(s) of cavity nucleation specific to titanium alloys, which include consideration of anisotropic plastic flow, are needed. This work, coupled with constrained-plasticity models for the early growth of submicron-size cavities, could provide better descriptions of the stress-state dependence of initiation compared to current phenomenological (external-work-based) approaches.

- Cavitation and fracture under industrial conditions: Industrial forming operations are typically non-isothermal and involve multiple processing steps/strain-path changes and variations in stress state across the section. Research to extend current damage-modeling capabilities to such TMP situations is needed. Two areas for which such work would be especially beneficial include the generation of cavities at the surface or center of large billets due to die chill or stress triaxiality, respectively. The kinetics of the formation of a metallurgical bond during cavity sealing would also be useful from both scientific and engineering standpoints.

- Multi-scale models for MTR elimination: To formulate process-design tools to minimize the retention of MTRs, basic research is needed to establish and couple (i) quantitative descriptions of sub-boundary evolution and local crystal rotations during the hot working of α/β titanium alloys with a colony-α microstructure and (ii) crystal-plasticity FEM (CPFEM) simulations. CPFEM methods would also be useful to quantify the deformation non-uniformity within individual colonies due to neighborhood effects and imposed macroscopic strains. By these means, the size and orientation of MTRs relative to subsequent service loading could be quantified.

- Coarse/abnormal β grain defects: To remedy such defects, quantitative models are needed to describe the effect of strain path, strain magnitude, and temperature on (i) the evolution of β-phase microtexture during α/β hot working and the early stages of β annealing and (ii) the evolution/persistence/number density of highly-misoriented β grains. This fundamental understanding should be incorporated into FEM simulations and mesoscale microstructure codes (*e.g.*, MC codes) to identify processing paths likely to give rise to coarse/abnormal grains. The

possible interaction between the kinetics and non-uniformity of dissolution of primary α [229] on the formation of a coarse-grain *vs* a grossly-abnormal β grain structure upon heating into the β phase field also warrants attention.

V. NOVEL PROCESSES

A number of TMP processes have been developed (or refined) to obtain novel microstructures and/or property combinations in α/β titanium alloys. These include those involving severe plastic deformation (SPD), rapid heat treatment, and solid-state joining.

A. *SPD Techniques for Ultrafine Microstructure*

Various large-deformation (also known as SPD) techniques have been applied to produce very fine microstructures in α/β titanium alloys such as Ti64. In many cases, these have involved warm working in the temperature range between approximately 873 and 1073 K (600 and 800 °C) *via* uniaxial or multiaxial ('abc') forging or plate/sheet rolling.[230–236] Methods such as equal-channel angular extrusion (ECAE) and high-pressure torsion (HPT) have also been utilized on a laboratory scale to establish the fundamental mechanisms of structure refinement and property enhancement.[237–240]

When interpreting the mechanical behavior of SPD-processed α/β titanium alloys, it is important to differentiate the microstructural features of α *particle* size and α *grain* size. In a formal sense, particle size refers to the α-phase entity delimited by α/β interphase boundaries. At moderate-to-high temperatures, α/β interface sliding is easy and thus controls superplastic deformation (Section II–C–1, Eq. [3]). Within each α particle, there may be α/α boundaries which determine the α grain/subgrain size; a fine α grain size can provide substantial Hall-Petch strengthening under ambient-temperature conditions. However, α/α boundaries do not generally contribute to superplastic flow because their sliding resistance is ~6 times that for sliding along α/β interfaces.[241] Because of the importance of α particle-*vs*-grain size, it is best to perform microstructure inspection *via* both SEM backscatter electron imaging and either EBSD or TEM. Unfortunately, it is rare to find such careful characterization in the literature.

Inagaki[234] and Zherebtsov *et al.*[242] were probably the first to demonstrate the importance of preform microstructure in obtaining a fine α particle size during warm SPD processing. Both demonstrated that a martensitic-/basketweave-α starting structure was best for obtaining a fine particle size during warm working. This finding can be ascribed to the ease of formation of subboundaries/shear bands during warm deformation of thin acicular microstructures and subsequent (dynamic or static) particle fragmentation. By contrast, a coarse lamellar starting structure was found to give rise to non-uniform mixtures of coarse and fine α particles; a preform structure of equiaxed α in a matrix of β led to

no α refinement. In these latter instances, the ease of subgrain formation within α particles likely precluded the formation of subboundaries intersecting α/β interfaces and thus particle fragmentation. Nevertheless, fine α *grain* sizes may be developed *via* warm working in such cases.

The benefit of martensitic-α in developing an ultrafine α grain size has also been demonstrated by Markovsky *et al.*[243] With this starting structure, they were able to produce a grain size of ~0.5 μm in Ti64 *via* a series of TMP cycles each consisting of warm deformation at ~873 K (600 °C) to a strain of only ~ 0.14 to 0.4 and an intermediate anneal of 5 minutes at 1023 K (800 °C).

The effect of α *grain size* on room-temperature strength has been determined for warm-rolled Ti64 samples having a partially- or fully- spheroidized starting microstructure.[235] In particular, it has been established that the yield-strength increment associated with grain size follows a Hall-Petch behavior (Figure 28).

The low-temperature superplasticity of warm-worked samples of Ti64 has also been investigated, but usually the α-particle size has not been reported. Two exceptions are the work of Semiatin *et al.*[152] and Zherebtsov *et al.*[156] in which the microstructure prior to warm working was martensitic α (*i.e.*, α′) Typical results from these two investigations are summarized in Table I. The total elongation in the former work was limited by crosshead travel, and thus is listed as >700 pct. Table I also summarizes results from other efforts in which Ti64 with a starting equiaxed-α structure was warm (or cold) worked, and subsequent low-temperature superplasticity was quantified. In these instances, however, only the α grain size after processing was reported. From a broad perspective, the data in the table reveal (i) Ti64 with a very fine α *grain size* (≤ 0.3 μm) may exhibit moderate strain-rate sensitivity (m ~0.2 to 0.5) and elongation (*e.g.*, 500 to 1000 pct.), and (ii) materials with a *particle size* which is much *larger* can have comparable or higher rate sensitivity and elongation. Nevertheless, all of the data do show a similar dependence of elongation (e_f) on m value (Figure 29). In this figure, the measurements from Table I are plotted and compared to predictions from an expression derived using a simple flow localization analysis[244]:

$$e_f = \left(1 - f_o^{l/m}\right)^{-m} - 1 \qquad [21]$$

in which e_f and f_o denote the elongation and the size of the initial geometric (or strength) inhomogeneity, respectively. The deviation from the model predictions (solid lines) for the point corresponding to the smallest value of m/elongation may be due to a failure that was fracture- rather than flow-localization controlled.

B. Rapid Heat Treatment

Rapid heat treatment of α/β titanium alloys can be used to develop refined and/or graded microstructures. Typically based on direct-resistance or induction heating, such techniques are usually limited to workpieces with a prismatic or relatively-simple cross-sectional geometry.

Perhaps the most common use of rapid heat treatment, β annealing involves *continuous* heating into the β phase field followed by rapid cooling.[245] By this means, a fine β grain size of ~50 to 100 μm can be obtained, thereby yielding a better combination of ductility and strength compared to furnace-heat-treated products having β grain sizes which are an order of magnitude larger. The two principal considerations in the design of rapid β annealing processes are (i) the effect of crystallographic texture on grain-growth kinetics *per se*, as described in Section III–C, and (ii) the rate of dissolution of the α phase and homogenization of α-stabilizing alloying elements. The latter aspects depend on the size and morphology of the primary- and secondary- α phases and heating rate and have been quantified using numerical techniques or measurements in the literature[229,246–248].

Another useful application is the *selective* heat treatment of parts for which the property requirements in various regions are different. For example, induction heating can be used to β anneal local areas of a component having an initially-uniform equiaxed-α microstructure to impart a transformed structure with enhanced creep or fatigue-crack-growth resistance.[249,250] The frequency and power level of the induction system and heating time are chosen based on the desired depth/extent of the beta-annealed/transformed layer. The development of a graded microstructure in α/β titanium alloys *via* this approach is often more cost effective than others involving the design of preforms with an initially-uniform structure of transformed β, which are forged and heat treated to convert local regions to an equiaxed-α structure.[251]

Recently, the conversion of the colony-α microstructure to an equiaxed one *via* the use of high-energy electropulsing has been reported.[252] Process parameters consisting of a frequency of 340 Hz, pulse duration of 80 μs, and current amplitude of ~250 A/mm² were used to transform a colony microstructure with 2-μm-thick lamellae into an equiaxed structure with 20-μm α particles. The peak temperatures developed during the process were only ~823 K (550 °C). Future work to reproduce these observations and elucidate the mechanism of the transformation is certainly warranted.
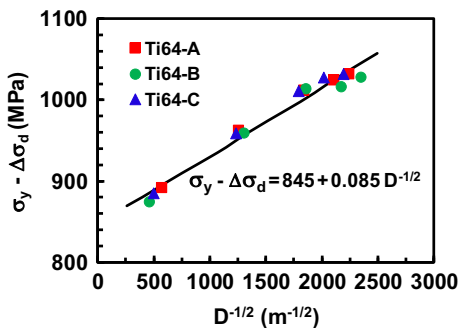
Fig. 28—Dependence of the yield strength (reduced by the contribution due to dislocations, Δσ_d) on the inverse-square-root of the α grain size for Ti64 samples which were warm rolled by various means.[235]

Table I. Measurements of Low-Temperature Superplasticity for Ti64

| Ref.	Preform Structure	Warm SPD Method	α Particle Size (μm)	α Grain Size (μm)	SP Temp (K)/Strain Rate (s^{-1})	m-Value	Elong. (Pct.)
152	α′	Rolling	1.88	—	$1048/10^{-4}, 10^{-3}$	0.62	700
156	α′	MAF* + Roll	~1	—	$823/10^{-4}$	0.45	1000
218	Equiax-α	MAF* + Roll	—	~ 0.3	$923/7 \times 10^{-3}$	0.34	690
218	Equiax-α	MAF* + Roll	—	~ 0.3	$973/7 \times 10^{-3}$	0.47	900
218	Equiax-α	MAF* + Roll	—	~ 0.3	$1023/7 \times 10^{-3}$	0.50	1100
239	Equiax-α	ECAE	—	~ 0.3	$973/10^{-4}$	0.35	475
241	Equiax-α	HPT	—	~ 0.04	$900/10^{-4}, 10^{-3}$	0.19	250
240	Equiax-α	HPT	—	~ 0.15	$923/10^{-3}$	0.37	575
242	Equiax-α	HPT	—	~ 0.15	$1000/10^{-2}$	0.4	505

MAF Multiaxial isothermal forge.
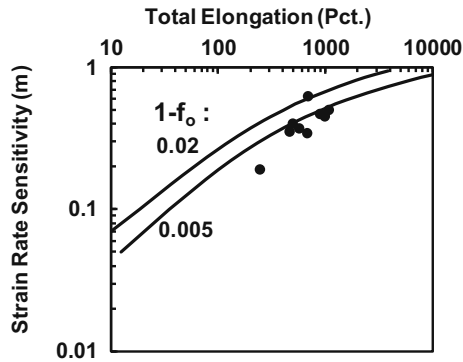
Fig. 29—Comparison of measurements (data points, Table I) of the total elongation as a function of the strain rate sensitivity (m value) of Ti64 samples with an ultrafine α grain size and model predictions (curves) based on Eq. [21] with two different values of the inhomogeneity factor 1−f$_o$.

C. Solid-State Joining Processes

Solid-state joining processes are typically broken into two broad categories- friction-stir welding (FSW) and rotary-/linear-friction welding (RFW/LFW).

FSW is used to join titanium sheet and plate products through the action of a rotating pin that translates along the seam between two workpieces. Key process variables comprise the rotation rate, traverse (feed) rate, and forging force. This leads to regions which are only heated (*i.e.*, a heat-affected zone), heated and deformed locally (a thermo-mechanically affected zone, or TMAZ, sometimes also referred as the transition zone), and heated and "stirred" (in which material undergoes gross deformation and motion around the FSW tool).

In α/β titanium alloys, a wide range of spatially-varying microstructures are produced by FSW. The specific microstructure is as a function of starting structure (*e.g.*, fully equiaxed, duplex, or fully lamellar) and the local strain, strain rate, and temperature (sub- or super-transus) experienced during the joining operation.[253–258] Local strains and strain rates in the stir region have been estimated *via* numerical modeling to reach as high as 100 and 1000 s^{-1}, respectively. For preform structures that are fully-equiaxed (mill-annealed) or duplex (equiaxed-α particles + secondary-α

platelets), regions that remain below the transus usually exhibit a mixture of α particles (with α grain sizes of the order of 1 to 3 μm) and colonies of secondary α. By contrast, process conditions that lead to a transient above the T$_β$ result in the formation of relatively-fine β grains with a size between ~10 and 40 μm, which is comparable to that developed during a corresponding supertransus rapid heat treatment. For workpieces that have an initial colony-α structure, FSW parameters that give rise to subtransus deformation leads to dynamic spheroidization by a mechanism similar to that described in Section III–E, resulting in equiaxed-α grains with a size of ~1 μm.[256]

One of the most useful applications of FSW of α/β titanium alloys has been the fabrication of *tailor-welded* blanks for subsequent sheet forming. In this regard, Sanders *et al.*[259] have demonstrated that proper selection of process variables during FSW can produce fine microstructures within and outside the weld nugget that enable uniform flow of the base metal and weld during subsequent superplastic sheet forming.

Linear-friction welding (LFW) is used primarily in the aerospace industry to join similar or dissimilar α/β titanium alloys. The process comprises the oscillatory rubbing of the mating ("faying") surfaces of two components subjected to a normal load to produce local heating.[260] Depending on process parameters and alloy/starting microstructure, material adjacent to the interface eventually becomes hot enough to deform plastically; this typically occurs at a temperature just below T$_β$.[261] The upsetting material flows outward (forming flash), thereby removing interfacial contaminants, bringing atomically clean surfaces into contact, and effecting a metallurgical bond. The microstructure at/near the weld tends to be fine, martensitic α whose texture shows noticeable α-variant selection during the decomposition of the high-temperature β phase.[261,262] In the adjacent, thermomechanically-affected and heat-affected zones, primary-α particles tend to show various degrees of elongation and the development of a fine internal structure suggestive of congruent and/or massive transformations during rapid heating and cooling cycles involved in friction joining[263] (Figure 30). Further work on the evolution of such unusual microstructural features and how they may be

manipulated to alter mechanical properties is highly warranted.

Several variants of FSW and LFW have been developed and applied to α/β titanium alloys. These include friction-stir *processing* (FSP) in which a rotating tool is used to introduce large deformations and thus refine the surface or local microstructure in the absence of joining *per se*. Second, asymmetric rolling of dissimilar sheet materials (*e.g.*, Ti64 and Ti17) has been shown to be capable of producing solid-state bonds as a result of high, local shear strains which enhance mechanical intermixing and inter-diffusion.[264]

VI. SUMMARY

Current understanding of various aspects of the thermomechanical processing (TMP) of α/β titanium alloys have been summarized in terms of hot-deformation behavior and the evolution of microstructure, texture, and defects. Hot deformation which provides the driving force for microstructure evolution tends to be complicated by the non-uniformity of plastic flow on both local and macroscopic scales, the presence of two phases with noticeably different flow properties, and phase size/morphology. Titanium alloys exhibit a rich variety of metallurgical phenomena whose mechanisms and kinetics can affect some aspect of primary, secondary, and finish processing. These include (i) dynamic/static recrystallization and grain growth in the β phase field and (ii) the decomposition of β during cooling and the fragmentation, spheroidization, and coarsening of the α phase during subtransus TMP steps. Such processes are confounded by plastic anisotropy and non-uniform flow that can result in defects such as cavities, retained microtexture regions, and abnormalities in grain structure.

Fundamental understanding of the metallurgical phenomena that control microstructure evolution during conventional mill processing and part manufacture has also been key in the development of a variety of novel processes. These include those that provide refined microstructure (enabling low-temperature superplastic deformation or enhanced strength in service), a novel or graded microstructure, reduced processing steps, improved joint integrity, *etc*.

A number of basic research opportunities have also been summarized in the area of TMP of α/β titanium alloys. The enhanced understanding that such work could provide may be of benefit not only for this alloy class, but for others, such as β titanium alloys, as well. In addition, the development and insertion of new titanium-synthesis and wrought processing techniques may be accelerated using fundamental understanding derived from the TMP of conventional (ingot-metallurgy) products. These newer approaches include so-called "meltless" titanium[265,266] in which titanium oxides are reduced directly without expensive intermediary steps (such as the production of $TiCl_4$); the methods yield a powder product that is consolidated by subsequent solid-state deformation processes. The formulation of new α/β Ti compositions that provide improved cold workability, thus enabling lower-cost production of thin-gage sheet products, is also a promising new technology for the titanium industry.[267]
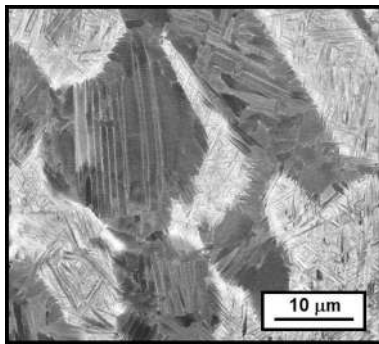
Fig. 30—Backscatter-electron image of the microstructure developed within the thermomechanically-affected zone during linear-friction welding of Ti64.[263]

REFERENCES

1. E.W. Collings: *The Physical Metallurgy of Titanium Alloys*, ASM International, Materials Park, OH, 1984.
2. G. Luetjering and J.C. Williams: *Titanium*, Springer, Berlin, 2007.
3. S.L. Semiatin, V. Seetharaman, and I. Weiss: *JOM*, 1997, vol. 49 (6), pp. 33–39.
4. S.L. Semiatin, V. Seetharaman, and I. Weiss: in *Advances in the Science and Technology of Titanium Alloy Processing*, I. Weiss, R. Srinivasan, P.J. Bania, D. Eylon, and S.L. Semiatin, eds., TMS, Warrendale, PA, 1997, pp. 3–73.
5. I. Weiss and S.L. Semiatin: *Mater. Sci. Eng. A*, 1998, vol. A243, pp. 46–65.
6. I. Weiss and S.L. Semiatin: *Mater. Sci. Eng. A*, 1999, vol. A263, pp. 243–56.
7. D. Banerjee, A.L. Pilchak, and J.C. Williams: *Mater. Sci. Forum*, 2012, vol. 710, pp. 66–84.
8. D. Banerjee and J.C. Williams: *Acta Mater.*, 2013, vol. 61, pp. 844–79.
9. R. Kolli and A. Devaraj: *Metals*, 2018, vol. 8 (7), pp. 506–546.
10. A.A. Salem and S.L. Semiatin: *Mater. Sci. Eng. A*, 2009, vol. A508, pp. 114–20.
11. J.C. Williams, R.G. Baggerly, and N.E. Paton: *Metall. Mater. Trans. A*, 2002, vol. 33A, pp. 837–50.
12. N. Gey, M. Humbert, M.J. Philippe, and Y. Combres: *Mater. Sci. Eng. A*, 1996, vol. A219, pp. 80–88.
13. M.G. Glavicic, P.A. Kobryn, R.L. Goetz, K.O. Yu, and S.L. Semiatin: in *Ti-2003: Science and Technology*, G. Lütjering and J. Albrecht, eds., Wiley-VCH Verlag GmbH, Weinheim, Germany, 2004, pp. 1299–306.
14. D. Dunst and H. Mecking: *Z. Metall.*, 1996, vol. 87, pp. 498–507.
15. S.L. Semiatin and T.R. Bieler: *Metall. Mater. Trans. A*, 2001, vol. 32A, pp. 1787–99.
16. M.L. Meier, D.R. Lesuer, and A.K. Mukherjee: *Mater. Sci. Eng. A*, 1991, vol. A136, pp. 71–78.
17. A. Arieli and A. Rosen: *Metall. Trans. A*, 1977, vol. 8A, pp. 1591–96.
18. J.A. Wert and N.E. Paton: *Metall. Trans. A*, 1983, vol. 14A, pp. 2535–44.
19. M. Tufts and C. Hammond: *Mater. Sci. Techn.*, 1999, vol. 15, pp. 1154–66.
20. G.A. Sargent, A.P. Zane, P.N. Fagin, A.K. Ghosh, and S.L. Semiatin: *Metall. Mater. Trans. A*, 2008, vol. 39A, pp. 2949–64.
21. S.L. Semiatin and G.D. Lahoti: *Metall. Trans. A*, 1981, vol. 12A, pp. 1705–17.
22. Y. Liu and T.N. Baker: *Mater. Sci. Eng. A*, 1995, vol. A197, pp. 125–31.
23. W-D. Zeng, Y-G. Zhou, and H-Q. Yu: in *Titanium '95: Science and Technology*, P.A. Blenkisop, W.J. Evans, and H.M. Flower, eds., The Institute of Materials, London, 1996, pp. 683–90.
24. R. Ding and Z.X. Guo: *Mater. Sci. Eng. A*, 2004, vol. A365, pp. 172–79.
25. M. Semblanet, L. Pallot, D. Piot, F. Montheillet, M. Derrien, Y. Millet, C. Poletti, and C. Desrayaud: in *Proc. 13th World Conference on Titanium*, V. Venkatesh, et al. eds., TMS, Warrandale, PA, 2016, pp. 689–94.
26. C. Poletti, L. Germain, F. Warchomicka, M. Dikovits, and S. Mitsche: *Mater. Sci. Eng. A*, 2016, vol. A651, pp. 280–90.
27. K. Hogrefe, R. Buzolin, and M.C. Poletti: in *Proc. 14th World Conference on Titanium*, 2019, in press.
28. T. Sheppard and J. Norley: *Met. Sci. Technol.*, 1988, vol. 4, pp. 903–08.
29. R. Buzolin, M. Lasnik, A. Krumphals, F. Krumphals, and M.C. Poletti: in *Proc. 14th World Conference on Titanium*, 2019, in press.
30. S. Gourdet and F. Montheillet: *Acta Mater.*, 2003, vol. 51, pp. 2685–99.
31. A. Majorell, S. Srivatsa, and R.C. Picu: *Mater. Sci. Eng. A*, 2002, vol. A326, pp. 297–305.
32. A. Elarbi, M. Jackson, and B. Wynnn: in *Proc. 12th World Conference on Titanium*, L. Zhou, H. Chang, Y. Lu, and D. Xu, eds., Science Press, Beijing, 2012, pp. 388–91.
33. P. Dadras, J.F. Thomas, Jr, and J.C. Moosbrugger: *Metall. Trans. A*, 1983, vol. 14A, pp. 1512–16.
34. S.L. Semiatin, V. Seetharaman, and I. Weiss: *Mater. Sci. Eng. A*, 1999, vol. A263, pp. 257–71.
35. E.B. Shell and S.L. Semiatin: *Metall. Mater. Trans. A*, 1999, vol. 30A, pp. 3219–29.
36. S.L. Semiatin and T.R. Bieler: *Acta Mater.*, 2001, vol. 49, pp. 3565–73.
37. X. Ma, W. Zeng, Y. Sun, K. Wang, Y. Lai, and Y. Zhou: *Mater. Sci. Eng. A*, 2012, vol. A538, pp. 182–89.
38. I. Balasundar, T. Raghu, and B.P. Kashyap: *Mater. Sci. Eng. A*, 2014, vol. A600, pp. 135–44.
39. P. Gao, H. Yang, X. Fan, and S. Zhu: *J. Alloys Comp.*, 2014, vol. 600, pp. 74–83.
40. C.H. Park, J.H. Kim, Y.-T. Hyun, J.-T. Yeom, and N.S. Reddy: *J. Alloys Comp.*, 2014, vol. 582, pp. 126–29.
41. R.M. Miller, T.R. Bieler, and S.L. Semiatin: *Scripta Mater.*, 1999, vol. 40, pp. 1387–93.
42. S.L. Semiatin and T.R. Bieler: *Metall. Mater. Trans. A*, 2001, vol. 32A, pp. 1871–75.
43. H. Oikawa and T. Oomori: *Mat. Sci. Eng. A*, 1988, vol. A104, pp. 125–30.
44. H. Oikawa: in *Metallurgy and Technology of Practical Titanium Alloys*, S. Fujishiro, D. Eylon, and T. Kishi, eds., TMS, Warrendale, PA, 1994, pp. 93–100.
45. H. Oikawa, Y. Ishikawa, and M. Seki: in *Titanium '92: Science and Technology*, F.H. Froes and I. Caplan, eds., TMS, Warrendale, PA, 1993, pp. 1779–86.
46. H. Oikawa, K. Nishimura, and M.X. Cui: *Scripta Metall.*, 1985, vol. 19, pp. 825–28.
47. P. Dadras and J.F. Thomas, Jr: *Metall. Trans. A*, 1981, vol. 12A, pp. 1867–76.
48. L. Briottet, J.J. Jonas, and F. Montheillet: *Acta Mater.*, 1996, vol. 44, pp. 1665–72.
49. S.L. Semiatin, F. Montheillet, G. Shen, and J.J. Jonas: *Metall. Mater. Trans. A*, 2002, vol. 33A, pp. 2719–27.
50. P. Vo, M. Jahazi, S. Yue, and P. Bocher: *Mater. Sci. Eng. A*, 2007, vol. A447, pp. 99–110.
51. J.H. Kim, S.L. Semiatin, Y.H. Lee, and C.S. Lee: *Metall. Mater. Trans. A*, 2011, vol. 42A, pp. 1805–14.
52. D. Dajno and F. Montheillet: *Colloque GS – Titane Traitements thermomécaniques*, Université Paris Sud, Paris, France, 1991, p. 67.
53. B. Vandecastele, N. Rizzi, and J.F. Wadier: in *Proc. Sixth World Titanium Conference*, P. Lacombe, R. Tricot, and G. Beranger, eds., Societe Francaise de Metallurgie, Les Ulis Cedex, France, 1988, pp. 1325–37.
54. S.L. Semiatin and T.R. Bieler: In *LiMAT-2001*, N.J. Kim, C.S. Lee, and D. Eylon, eds., Pohang University of Science and Technology, Pohang, Korea, 2001, pp. 79–90.
55. R.A. Lebensohn and G.R. Canova: *Acta Mater.*, 1997, vol. 45, pp. 3687–94.
56. J.E. Bird, A.K. Mukherjee, and J. E. Dorn in: *Quantitative Relation Between Microstructure and Properties*, D.G. Brandon and A. Rosen, eds., Israel Universities Press, Jerusalem, Israel, 1969, pp. 255–342.
57. T.G. Langdon: *J. Mater. Sci.*, 2006, vol. 41, pp. 597–609.
58. E. Alabort, P. Kontis, D. Barba, K. Dragnevski, and R.C. Reed: *Acta Mater.*, 2016, vol. 105, pp. 449–63.
59. S.L. Semiatin and G.A. Sargent: *Key Eng. Mater.*, 2010, vol. 433, pp. 235–40.
60. A. Laasraoui and J.J. Jonas: *Metall. Trans.*, 1991, vol. 22A, pp. 1545–60.
61. F. Montheillet, D. Piot, N. Matougui, and M.L. Fares: *Metall. Mater. Trans. A*, 2014, vol. 45A, pp. 4324–32.
62. Y. Estrin and H. Mecking: *Acta Metall.*, 1984, vol. 32, pp. 57–70.
63. H. Liang, H. Guo, Y. Nan, C. Qin, X. Peng, and J. Zhang: *Mater. Sci. Eng. A*, 2014, vol. A615, pp. 42–50.
64. P.M. Souza, H. Beladi, R. Singh, B. Rolfe, and P.D. Hodgson: *Mater. Sci. Eng. A*, 2015, vol. A648, pp. 265–73.
65. X.G. Fan, H. Yang, Z.C. Sun, and D.W. Zhang: in *Proc. 12th World Conference on Titanium*, L. Zhou, H. Chang, Y. Lu, and D. Xu, eds., Science Press, Beijing, 2012, pp. 324–27.
66. R.C. Picu and A. Majorell: *Mater. Sci. Eng. A*, 2002, vol. A326, pp. 306–16.
67. B. Babu and L.-E. Lindgren: *Int. J. Plasticity*, 2013, vol. 50, pp. 94–108.

68. S.S. Babu, J. Livingston, and J.C. Lippold: *Metall. Mater. Trans. A*, 2013, vol. 44A, pp. 3577–91.
69. M. Saby, E. Massoni, and N. Bozzolo: *Mater. Characterization*, 2014, pp. 88–92.
70. S.L. Semiatin, N.C. Levkulich, C.A. Heck, A.E. Mann, N. Bozzolo, A.L. Pilchak, and J.S. Tiley: *Metall. Mater. Trans. A*, 2020, vol. 51A, in press.
71. I. Weiss and F.H. Froes: in *Titanium '84: Science and Technology*, G. Luetjering, U. Zwicker, and W. Bunk, eds., Deutsche Gesellschaft fur Metallkunde E.V., Oberursel, Germany, 1985, pp. 499–506.
72. F. Chaussy and J.H. Driver: in *Beta Titanium Alloys*, A. Vassel, D. Eylon, and Y. Combres, eds., Editions de la Revue de Metallurgie, Paris, 1994, pp. 57–64.
73. R. Ding, Z.X. Guo, and A. Wilson: *Mater. Sci. Eng. A*, 2002, vol. A327, pp. 233–45.
74. P. Vo, M. Jahazi, and S. Yue: *Metall. Mater. Trans. A*, 2008, vol. 39A, pp. 2965–80.
75. T. Furuhara, Y. Toji, and T. Maki: in *Ti-2003: Science and Technology*, G. Lütjering and J. Albrecht, eds., Wiley-VCH Verlag GmbH, Weinheim, Germany, 2004, pp. 1219–26.
76. T. Furuhara, B. Poorganji, H. Abe, and T. Maki: *JOM*, 2007, vol. 59 (1), pp. 64–67.
77. D.L. OuYang, M.W. Fu, and S.Q. Lu: *Mater. Sci. Eng. A*, 2014, vol. A619, pp. 26–34.
78. B. Derby: *Acta Metall. Mater.*, 1991, vol. 39, pp. 955–62.
79. T. Seshacharyulu, S.C. Medeiros, W.G. Frazier, and Y.V.R.K. Prasad: *Mater. Sci. Eng. A*, 2002, vol. A325, pp. 112–25.
80. L. Pallot, PhD Thesis, Ecole Nationale des Mines de Saint-Etienne, Saint-Etienne, France, 2012.
81. F. Chaussy: PhD Thesis, Institut National Polytechnique de Grenoble, Grenoble, France, 1996.
82. N. Come-Dingremont, E. Gautier, and A. Simon: in *Titanium '92: Science and Technology*, F.H. Froes and I.L. Caplan, eds, TMS, Warrendale, PA, 1993, pp. 667–74.
83. J.M. Kempf, E. Gautier, A. Simon, J.F. Uginet, and A. Gavart: in *Titanium '92: Science and Technology*, F.H. Froes and I.L. Caplan, eds, TMS, Warrendale, PA, 1993, pp. 627–34.
84. A. Krumphals, M. Stockinger, F. Warchomicka, and C. Sommitsch: : in *Proc. 12th World Conference on Titanium*, L. Zhou, H. Chang, Y. Lu, and D. Xu, eds., Science Press, Beijing, 2012, pp. 493–96.
85. L.A. Elagina, A.I. Gordienko, O.P. Evmenov, and V.V. Ivashko: in *Titanium and Titanium Alloys: Scientific and Technological Aspects*, J.C. Williams and A.F. Belov, eds, Plenum Press, New York, 1982, pp. 1789–98.
86. M. Semblanet, F. Montheillet, D. Piot, C. Desrayaud, A. Beneteau, and Y. Millet: in *Proc. 12th World Conference on Titanium*, L. Zhou, H. Chang, Y. Lu, and D. Xu, eds., Science Press, Beijing, 2012, pp. 573–76.
87. M. Allan, M. Thomas, J. Brooks, and P. Blackwell: in *Proc. 13th World Conference on Titanium*, V. Venkatesh, et al. eds., TMS, Warrandale, PA, 2016, pp. 203–08.
88. A.L. Pilchak, G.A. Sargent, and S.L. Semiatin: *Metall. Mater. Trans. A*, 2018, vol. 49A, pp. 908–19.
89. S.P. Fox: in *Titanium'92: Science and Technology*, F.H. Froes and I.L. Caplan, eds., TMS, Warrendale, PA, 1993, pp. 769–76.
90. F.J. Gil, P. Tarin, and J.A. Planell: in *Titanium'92: Science and Technology*, F.H. Froes and I.L. Caplan, eds., TMS, Warrendale, PA, 1993, pp. 777–84.
91. O.M. Ivasishin, S.V. Shevchenko, and S.L. Semiatin: *Mater. Sci. Eng. A*, 2002, vol. A332, pp. 343–50.
92. S.L. Semiatin, P.N. Fagin, M.G. Glavicic, I.M. Sukonnik, and O.M. Ivasishin: *Mater. Sci. Eng. A*, 2001, vol. A299, pp. 225–34.
93. O.M. Ivasishin, S.L. Semiatin, P.E. Markovsky, S.V. Shevchenko, and S.V. Ulshin: *Mater. Sci. Eng. A*, 2002, vol. A337, pp. 88–96.
94. G. Abbruzzese and K. Lucke: *Acta Metall.*, 1986, vol. 34, pp. 905–14.
95. H. Eichelkraut, G. Abbruzzese, and K. Lucke: *Acta Metall.*, 1988, vol. 36, pp. 55–68.
96. O.M. Ivasishin, S.V. Shevchenko, N.L. Vasiliev, and S.L. Semiatin: *Acta Mater.*, 2003, vol. 51, pp. 1019–34.
97. O.M. Ivasishin, S.V. Shevchenko, P.E. Markovsky, and S.L. Semiatin: in *Ti-2003: Science and Technology*, G. Luetjering and J. Albrecht, eds., Wiley-VCH Verlag GmbH, Weinheim, Germany, 2004, pp. 1307–14.
98. N. Ma, A. Kazaryan, S.A. Dregia, and Y. Wang: *Acta Mater.*, 2004, vol. 52, pp. 3869–79.
99. S.P. Fox and D.F. Neal: in *Titanium '95: Science and Technology*, P.A. Blenkisop, W.J. Evans, and H.M. Flower, eds., The Institute of Materials, London, 1996, pp. 628–35.
100. F.J. Gil, M.P. Ginebra, J.M. Manero, and J.A. Planell: *J. Alloys Compd.*, 2001, vol. 329, pp. 142–52.
101. S. Malinov, P. Markovsky, W. Sha, and Z. Guo: *J. Alloys Compd.*, 2001, vol. 314, pp. 181–92.
102. S. Malinov, Z. Guo, W. Sha, and A. Wilson: *Metall. Mater. Trans. A*, 2001, vol. 32A, pp. 879–87.
103. I. Katzarov, S. Malinov, and W. Sha: *Metall. Mater. Trans. A*, 2002, vol. 33A, pp. 1027–40.
104. R. Shi, D. Wang, and Y. Wang: in *ASM Handbook*, Vol. 4E, G.E. Totten and D.S. McKenzie, eds., ASM International, Materials Park, OH, 2016, pp. 573–603.
105. G. Lutjering: *Mater. Sci. Eng. A*, 1998, vol. A243, pp. 32–45.
106. M. Meng, H.G. Fan, H. Yang, L.G. Guo, M. Zhan, and P.F. Gao: *J. Alloys Compd.*, 2017, vol. 714, pp. 294–302.
107. H.J.G. Gundersen, T.B. Jensen, and R. Osterby: *J. Microsc*, 1978, vol. 113 (Part 1), pp. 27–43.
108. N. Stefansson and S.L. Semiatin: *Metall. Mater. Trans. A*, 2003, vol. 34A, pp. 691–98.
109. T. Searles, J. Tiley, A. Tanner, R. Williams, B. Rollins, E. Lee, S. Kar, R. Banerjee, and H.L. Fraser: *Meas. Sci. Technol.*, 2005, vol. 16, pp. 60–69.
110. H. Sharma, S.M.C van Bohemen, R.H. Petrov, and J. Sietsma: *Acta Mater.*, 2010, vol. 58, pp. 2399–407.
111. E. Wielewski, D.B. Menasche, P.G. Callahan, and R.M. Suter: *J. Appl. Crystallogr.*, 2015, vol. 48, pp. 1165–71.
112. S.L. Semiatin and P.S. Poteet: *Metall. Mater. Trans. A*, 2008, vol. 39A, pp. 2538–41.
113. D.J. Li, P.A. Russo, K.O. Yu, J.M. Hjelm, and G.W. Kuhlman: in *Proc. Thermec 2000*, T. Chandra, K. Higashi, C. Suryanarayana, and C. Tome, eds., Elsevier Science Ltd., Amsterdam, The Netherlands, 2001.
114. V. Venkatesh and A.F. Wilson: in *Ti-2007: Science and Technology*, M. Ninomi, S. Akiyama, M. Ikeda, M. Hagiwara, and K. Maruyama, eds, Japan Institute of Metals, Sendai, Japan, 2007, pp. 865–68.
115. V. Venkatesh, A. Wilson, M. Kamal, M. Thomas, and D. Lambert: *JOM*, 2009, vol. 61 (5), pp. 45–50.
116. H. Margolin and P. Cohen: in *Titanium '80: Science and Technology*, H. Kimura and O. Izumi, eds., TMS, Warrendale, PA, 1980, pp. 1555–61.
117. I. Weiss, G.E. Welsch, F.H. Froes, and D. Eylon: in *Titanium: Science and Technology*, G. Luetjering, U. Zwicker, and W. Bunk, eds., Deutsche Gesellschaft fur Metallkunde e.V., Oberursel, Germany, 1985, pp. 1503–10.
118. I. Weiss, F.H. Froes, D. Eylon, and G.E. Welsch: *Metall. Trans. A*, 1986, vol. 17A, pp. 1935–47.
119. G. Welsch, I. Weiss, D. Eylon, and F.H. Froes: in *Advances in the Science and Technology of Titanium Alloy Processing*, I. Weiss, R. Srinivasan, P.J. Bania, D. Eylon, and S.L. Semiatin, eds., TMS, Warrendale, PA, 1997, pp. 169–83.
120. W.W. Mullins: *Trans. TMS-AIME*, 1960, vol. 218, pp. 354–61.
121. S.L. Semiatin and D.U. Furrer: in *ASM Handbook*, Vol. 22A, Tenth Edition, D.U. Furrer and S.L. Semiatin, eds., ASM International, Materials Park, OH, 2009, pp. 522–35.
122. S. Zherebtsov, M. Murzinova, G. Salishchev, and S.L. Semiatin: *Acta Mater.*, 2011, vol. 59, pp. 4138–50.
123. G.A. Salishchev, S.V. Zherebtsov, S.Yu. Mironov, and S.L. Semiatin: *Mater. Sci. Forum*, 2004, vols. 467–470, pp. 501–06.
124. S. Mironov, M. Murzinova, S. Zherebtsov, G.A. Salishchev, and S.L. Semiatin: *Acta Mater.*, 2009, vol. 57, pp. 2470–81.
125. Y. Ito, S. Murakami, and N. Tsuji: *Metall. Mater. Trans. A*, 2017, vol. 48A, pp. 4237–46.
126. S.A.A. Shams, S. Mirdamadi, S.M. Abbasi, D. Kim, and C.S. Lee: *Metall. Mater. Trans. A*, 2017, vol. 48A, pp. 2979–92.

127. B. Poorganji, M. Yamaguchi, Y. Itsumi, K. Matsumoto, T. Tanaka, Y. Asa, G. Miyamoto, and T. Furuhara: *Scripta Mater.*, 2009, vol. 61, pp. 419–22.
128. H. Matsumoto, L. Bin, S.-H. Lee, Y. Li, Y. Ono, and A. Chiba: *Metall. Mater. Trans. A*, 2013, vol. 44A, pp. 3245–60.
129. S. Zherebtsov, G.A. Salishchev, and S.L. Semiatin: *Philos. Mag. Letters*, 2010, vol. 90 (12), pp. 903–14.
130. M. Klimova, S. Zherebtsov, G. Salishchev, and S.L. Semiatin: *Mater Sci. Eng. A*, 2015, vol. A645, pp. 292–97.
131. K. Muszka, M. Lopez-Pedrosa, K. Raszka, M. Thomas, W.M. Rainforth, and B.P. Wynne: *Metall. Mater. Trans. A*, 2014, vol. 45A, pp. 5997–6007.
132. S.L. Semiatin, J.F. Thomas, and P. Dadras: *Metall. Trans. A*, 1983, vol. 14A, pp. 2363–74.
133. S. Roy and S. Suwas: *J. Alloys Compd.*, 2013, vol. 548, pp. 110–25.
134. B. Perumal, M.A. Rist, S. Gungor, J.W. Brooks, and M.E. Fitzpatrick: *Metall. Mater. Trans. A*, 2016, vol. 47A, pp. 4128–36.
135. T.R. Bieler and S.L. Semiatin: *Int. J. Plasticity*, 2002, vol. 18, pp. 1165–89.
136. S. Suri, G.B. Viswanathan, T. Neeraj, D.H. Hou, and M.J. Mills: *Acta Mater.*, 1999, vol. 47, pp. 1019–34.
137. H.-W. Song, S.-H. Zhang, and M. Cheng: *J. Alloys Compd.*, 2009, vol. 480, pp. 922–27.
138. K. Wang, W. Zeng, Y. Zhao, Y. Lai, and Y. Zhou: *Mater. Sci. Eng. A*, 2010, vol. A527, pp. 2559–66.
139. X. Ma, W. Zeng, F. Tian, and Y. Zhou: *Mater. Sci. Eng. A*, 2012, vol. A548, pp. 6–11.
140. A.A. Korshunov, F.U. Enikeev, M.I. Mazurskii, G.A. Salishchev, A.V. Muravlev, P.V. Chistyakov, and O.O. Dimitriev: *Russ. Metall.*, 1994, vol. 3, pp. 103–08.
141. R.M. Poths, G. Angella, B.P. Wynn, W.M. Rainforth, S.L. Semiatin, and J.H. Beynon: *Metall. Mater. Trans. A*, 2004, vol. 35A, pp. 2993–3001.
142. P.D. Nicolaou and S.L. Semiatin: *Metall. Mater. Trans. A*, 2007, vol. 38A, pp. 3023–31.
143. S.L. Semiatin, N. Stefansson, and R.D. Doherty: *Metall. Mater. Trans. A*, 2005, vol. 36A, pp. 1372–76.
144. T.H. Courtney and J.C. Malzahn Kampe: *Acta Metall.*, 1989, vol. 37, pp. 1747–58.
145. C.H. Park, J.W. Won, J.-W. Park, S.L. Semiatin, and C.S. Lee: *Metall. Mater. Trans. A*, 2012, vol. 43A, pp. 977–85.
146. C.H. Park, S.-W. Kim, C.-S. Oh, Y.-T. Hyun, J.-K. Hong, and J.-T. Yeom: *Philos. Mag. Lett.*, 2012, vol. 92 (12), pp. 701–09.
147. S. Roy and S. Suwas: *Acta Mater.*, 2017, vol. 134, pp. 283–301.
148. S. Roy and S. Suwas: *Scripta Mater.*, 2018, vol. 154, pp. 1–7.
149. P.G.K. Amos, E. Schoof, D. Schneider, and B. Nestler: *Acta Mater.*, 2018, vol. 159, pp. 51–64.
150. N. Stefansson, S.L. Semiatin, and D. Eylon: *Metall. Mater. Trans. A*, 2002, vol. 33A, pp. 3527–34.
151. S.L. Semiatin, B.C. Kirby, and G.A. Salishchev: *Metall. Mater. Trans. A*, 2004, vol. 35A, pp. 2809–19.
152. S.L. Semiatin, P.N. Fagin, J.F. Betten, A. Zane, A.K. Ghosh, and G.A. Sargent: *Metall. Mater. Trans. A*, 2010, vol. 41A, pp. 499–512.
153. C.H. Park, B. Lee, S.L. Semiatin, and C.S. Lee: *Mater. Sci. Eng. A*, 2010, vol. A527, pp. 5203–11.
154. S.L. Semiatin, F. Sun, E. Crist, K.O. Yu, G.A. Sargent, and D.G. Sanders: *Metall. Mater. Trans. A*, 2016, vol. 47A, pp. 4374–77.
155. J.W. Martin, R.D. Doherty, and B. Cantor: *Stability of Microstructure in Metallic Systems*, Cambridge University Press, Cambridge, 1997.
156. S. Zherebtsov, E. Kudrjavtsev, G. Salishchev, B.B. Straumal, and S.L. Semiatin: *Acta Mater.*, 2016, vol. 121, pp. 152–63.
157. S.L. Semiatin, M.W. Corbett, P.N. Fagin, G.A. Salishchev, and C.S. Lee: *Metall. Mater. Trans. A*, 2006, vol. 37A, pp. 1125–36.
158. J.C. Williams and E.A. Starke, Jr.: in *Deformation, Processing, and Structure*, G. Krauss, ed., ASM International, Materials Park, OH, 1984, pp. 279–354.
159. M. Peters and G. Luetjering: in *Titanium '80: Science and Technology*, H. Kimura and O. Izumi, eds., TMS, Warrendale, PA, 1980, pp. 925–35.
160. S.L. Semiatin, S.V. Shevchenko, O.M. Ivasishin, M.G. Glavicic, Y.B. Chun, and S.K. Hwang: in *ASM Handbook*, Vol. 22A, Tenth Edition, D.U. Furrer and S.L. Semiatin, eds., ASM International, Materials Park, OH, 2009, pp. 536–52.
161. A.K. Singh and R.A. Schwarzer: *Trans. Indian Inst. Met.*, 2008, vol. 61, pp. 371–87.
162. M.G. Glavicic, P.A. Kobryn, R.L. Goetz, K.O. Yu, and S.L. Semiatin: in *Ti-2003: Science and Technology*, G. Lütjering and J. Albrecht, eds., Wiley-VCH Verlag GmbH, Weinheim, 2004, pp. 1299–306.
163. M.G. Glavicic, R.L. Goetz, D.R. Barker, G. Shen, D. Furrer, A. Woodfield, and S.L. Semiatin: *Metall. Mater. Trans. A*, 2008, vol. 39A, pp. 887–96.
164. N.R. Barton and P.R. Dawson: *Model. Simul. Mater. Sci. Eng.*, 2001, vol. 9, pp. 433–63.
165. N. Stanford and P.S. Bate: *Acta Mater.*, 2004, vol. 52, pp. 5215–24.
166. G.C. Obasi, S. Birosca, J. Quinta da Fonseca, and M. Preuss: *Acta Mater.*, 2012, vol. 60, pp. 1048–58.
167. D. Bhattacharyya, G.B. Viswanathan, R. Denkenberger, D. Furrer, and H.L. Fraser: *Acta Mater.*, 2003, vol. 51, pp. 4679–91.
168. G.C. Obasi, S. Birosca, D.G. Leo Prakash, J. Quinta da Fonseca, and M. Preuss: *Acta Mater.*, 2012, vol. 60, pp. 6013–24.
169. G.C. Obasi, S. Birosca, D.G. Leo Prakash, J. Quinta da Fonseca, and M. Preuss: in *Proc. 12th World Conference on Titanium*, L. Zhou, H. Chang, Y. Lu, and D. Xu, eds., Science Press, Beijing, 2012, pp. 771–75.
170. H. Moustahfid, N. Gey, M. Humbert, and M.J. Philippe: *Metall. Mater. Trans. A*, 1997, vol. 28A, pp. 51–59.
171. N. Gey, M. Humbert, M.J. Philippe, and Y. Combres: *Mater. Sci. Eng. A*, 1997, vol. A230, pp. 68–74.
172. R. Shi, N. Zhou, S.R. Niezgoda, and Y. Wang: *Acta Mater.*, 2015, vol. 94, pp. 224–43.
173. G.A. Sargent, K.T. Kinsel, A.L. Pilchak, A.A. Salem, and S.L. Semiatin: *Metall. Mater. Trans. A*, 2012, vol. 43A, pp. 3570–85.
174. A.W. Bowen: *Mater. Sci. Eng.*, 1977, vol. 29, pp. 19–28.
175. S.V. Divinski, V.N. Dnieprenko, and O.M. Ivasishin: *Mater. Sci. Eng. A*, 1998, vol. A243, pp. 201–05.
176. J.L.W. Warwick, N.G. Jones, I. Bantounas, M. Preuss, and D. Dye: *Acta Mater.*, 2013, vol. 61, pp. 1603–15.
177. M. Humbert, L. Germaine, N. Gey, P. Bocher, and M. Jahazi: *Mater. Sci. Eng. A*, 2006, vol. A430, pp. 157–64.
178. L. Zeng and T.R. Bieler: *Mater. Sci. Eng. A*, 2005, vol. A392, pp. 403–14.
179. J. Koike, Y. Shimoyama, I. Ohnuma, T. Okamura, R. Kainuma, K. Ishida, and K. Maruyama: *Acta Mater.*, 2000, vol. 48, pp. 2059–69.
180. B. Guo, S.L. Semiatin, J. Liang, B. Sun, and J.J. Jonas: *Metall. Mater. Trans. A*, 2018, vol. 49A, pp. 1450–54.
181. B. Guo, C. Aranas, A. Foul, X. Ji, A. Fall, M. Jahazi, and J.J. Jonas: *Mater. Sci. Eng. A*, 2018, vol. A729, pp. 119–24.
182. J.S. Jha, B. Jayabalan, S.P. Toppo, R. Singh, A. Tewari, and S.K. Mishra: *Philos. Mag.*, 2019, vol. 99, pp. 1429–59.
183. S. Balachandran, S. Kumar, and D. Banerjee: *Acta Mater.*, 2017, vol. 131, pp. 423–34.
184. S.L. Semiatin: in *Handbook of Workability and Process Design*, G.E. Dieter, H.A. Kuhn, and S.L. Semiatin, eds., ASM International, Materials Park, OH, 2003, chap. 13.
185. H. Fujii and H.G. Suzuki: *Scripta Metall.*, 1990, vol. 24, pp. 1843–46.
186. H. Suzuki and D. Eylon: *ISIJ Int.*, 1993, vol. 33, pp. 1270–74.
187. H. Suzuki and D. Eylon: *Mater. Sci. Eng. A*, 1998, vol. A243, pp. 126–33.
188. B.B. Rath, B.K. Damkroger, M.A. Imam, and G.R. Edwards: *Report SAND-94-0283C (CONF-940221-3)*, Sandia National Laboratories, Sandia, NM, 1994.
189. S.L. Semiatin, V. Seetharaman, A.K. Ghosh, E.B. Shell, M.P. Simon, and P.N. Fagin: *Mater. Sci. Eng. A*, 1998, vol. A256, pp. 92–110.
190. S.L. Semiatin, R.L. Goetz, E.B. Shell, V. Seetharaman, and A.K. Ghosh: *Metall. Mater. Trans. A*, 1999, vol. 30A, pp. 1411–24.
191. M.G. Cockcroft and D.J. Latham: *J. Inst. Met.*, 1958, vol. 96, pp. 33–39.

192. P.D. Nicolaou, R.L. Goetz, J.D. Miller, and S.L. Semiatin: *Metall. Mater. Trans. A*, 2003, vol. 34A, pp. 2397–400.
193. V. Venkatesh and S.P. Fox: in *Microstructure Modeling and Prediction during Thermomechanical Processing*, R. Srinivasan, S.L. Semiatin, A. Beaudoin, S.P. Fox, and Z. Jin, eds., TMS, Warrendale, PA, 2001, pp. 147–56.
194. A.K. Ghosh, D.-H. Bae, and S.L. Semiatin: *Mater. Sci. Forum*, 1999, vol. 304/306, pp. 609–15.
195. A.K. Ghosh, D.-H. Bae, and S.L. Semiatin: *ASM Handbook*, ASM International, Materials Park, OH, 2009, vol. 22A, pp. 339–52.
196. J.W. Hancock: *Metal Sci.*, 1976, pp. 319–25.
197. P.D. Nicolaou, A.K. Ghosh, and S.L. Semiatin: *ASM Handbook*, ASM International, Materials Park, OH, 2009, vol. 22A, pp. 325–38.
198. T.R. Bieler, P.D. Nicolaou, and S.L. Semiatin: *Metall. Mater. Trans. A*, 2005, vol. 36A, pp. 129–40.
199. T.R. Bieler, M.G. Glavicic, and S.L. Semiatin: *JOM*, 2002, vol. 54 (1), pp. 31–36.
200. P.D. Nicolaou, J.D. Miller, and S.L. Semiatin: *Metall. Mater. Trans. A*, 2005, vol. 36A, pp. 3461–70.
201. P.D. Nicolaou and S.L. Semiatin: *Metall. Mater. Trans. A*, 2005, vol. 36A, pp. 1567–74.
202. P.D. Nicolaou and S.L. Semiatin: *Metall. Mater. Trans. A*, 2006, vol. 37A, pp. 3697–705.
203. P.D. Nicolaou, R.L. Goetz, and S.L. Semiatin: *Metall. Mater. Trans. A*, 2008, vol. 39A, pp. 659–65.
204. M. Saby, P.O. Bouchard, and M. Bernacki: *Finite Elements Anal Design*, 2015, vol. 105, pp. 63–78.
205. B. Derby and E.R. Wallach: *Metal Sci.*, 1982, vol. 16, pp. 49–56.
206. A.P. Woodfield, M.D. Gorman, R.R. Corderman, J.A. Sutliff, and B. Yamrom: in *Titanium '95: Science and Technology*, P.A. Blenkisop, W.J. Evans, and H.M. Flower, eds., The Institute of Materials, London, 1996,1116–23.
207. C.J. Scezpanski, J.M. Larsen, and S.L. Semiatin: Air Force Research Laboratory, Unpublished Research, Wright-Patterson Air Force Base, OH, 2010.
208. A.L. Pilchak, C.J. Szczepanski, J.A. Shaffer, A.A. Salem, and S.L. Semiatin: *Metall. Mater. Trans. A*, 2013, vol. 44A, pp. 4881–90.
209. C.J. Szczepanski, S.K. Jha, J.M. Larsen, and J.W. Jones: *Metall. Mater, Trans. A*, 2008, vol. 39A, pp. 2841–51.
210. A.L. Pilchak and J.C. Williams: *Metall. Mater. Trans. A*, 2011, vol. 42A, pp. 1000–27.
211. L. Germain, N. Gey, M. Humbert, P. Vo, M. Jahazi, and P. Bocher: *Acta Mater.*, 2008, vol. 56, pp. 4298–308.
212. I. Bantounas, D. Dye, and T.C. Lindley: *Acta Mater.*, 2010, vol. 58, pp. 3908–18.
213. L. Germain, N. Gey, M. Humbert, P. Bocher, and M. Jahazi: *Acta Mater.*, 2005, vol. 53, pp. 3535–43.
214. N. Gey, P. Bocher, E. Uta, L. Germain, and M. Humbert: *Acta Mater.*, 2012, vol. 60, pp. 2647–55.
215. G.A. Salishchev, O.R. Valiakhmetov, and R.M. Galeyev: *J. Mater. Sci.*, 1993, vol. 28, pp. 2898–902.
216. G.A. Salishchev, R.M. Galeyev, O.R. Valiakhmetov, R.V. Safiullin, R.Y. Lutfullin, O.N. Senkov, F.H. Froes, and O.A. Kaibyshev: *J. Mater. Proc. Technol.*, 2001, vol. 116, pp. 265–68.
217. G.A. Salischev, S.Yu. Mironov, and S.V. Zherebtsov: *Rev. Adv. Mater. Sci.*, 2006, vol. 11, pp. 152–58.
218. M.D. Gorman, A.P. Woodfield, and B. A. Link: US Patent 6,284,070, September 4, 2001.
219. M.F.X. Gigliotti, R.S. Gilmore, J.B. Deaton, Jr., and J.A. Sutliff: US Patent 6,401,537, June 11, 2002.
220. A.P. Woodfield: US Patent 6,918,974, July 19, 2005.
221. B.P. Bewlay, M.F.X. Gigliotti, Jr., D.U. Furrer, G. Shen, and J.M. Franczak: US Patent 6,387,197, 2002.
222. R. Ma, A.L. Pilchak, S.L. Semiatin, and T.J. Truster: *Int. J. Plasticity*, 2018, vol. 107, pp. 189–206.
223. F.J. Humphreys: *Acta Mater.*, 1997, vol. 45, pp. 4231–40.
224. D. Raabe, F. Roters, and V. Marx: *Textures Microstruct*, 1996, vols. 26–27, pp. 611–35.
225. A.L. Pilchak, S. Srivatsa, N.C. Levkulich, V. Sinha, E.J. Payton, and S.L. Semiatin: in *Proc. 14th World Conference on Titanium*, 2019, in press.
226. N.E. Byres, J. Quinta da Fonseca, B. Dod, and P.B. Prangnell: in *Proc. 14th World Conference on Titanium*, 2019, in press.
227. D. Solas, A. Paris, A.L. Helbert, T. Baudin, F. Brisset, B. Dod, and R. Forestier: in *Proc.14th World Conference on Titanium*, 2019, in press.
228. O.M. Ivasishin, S.V. Shevchenko, and S.L. Semiatin: *Scripta Mater.*, 2004, vol. 50, pp. 1241–45.
229. S.L. Semiatin, M. Obstalecki, E.J. Payton, A.L. Pilchak, P.A. Shade, N.C. Levkulich, J.M. Shank, D.C. Pagan, F. Zhang, and J.S. Tiley: *Metall. Mater. Trans. A*, 2019, vol. 50A, pp. 2356–70.
230. H. Garbacz, I.P. Semenova, S. Zherebtsov, and M. Motyka, eds.: *Nanocrystalline Titanium*, Elsevier, Amsterdam, 2019.
231. G.A. Salishchev, S.V. Zherebtsov, O.R. Valiakhmetov, R.M. Galeyev, V.K. Berdin, and S.L. Semiatin: in *Ti-2003: Science and Technology*, G. Luetjering and J. Albrecht, eds., Wiley-VCH Verlag GmbH, Weinheim, 2004, pp. 313–20.
232. S. Zherebtsov, S. Mironov, M. Murzinova, G. Salishchev, and S.L. Semiatin: *Mater. Sci. Forum*, 2008, vols. 584–586, pp. 771–76.
233. C.H. Park, Y.G. Ko, J.-W. Park, and C.S. Lee: *Mater. Sci. Eng. A*, 2008, vol. A496, pp. 150–58.
234. H. Inagaki: *Z. Metall.*, 1995, vol. 86, pp. 643–50.
235. Z. Li, Y. Sun, E.J. Lavernia, and A. Shan: *Metall. Mater. Trans. A*, 2015, vol. 46A, pp. 5047–57.
236. S.V.S.N. Murty, N. Nayan, P. Kumar, P.R. Narayanan, S.C. Sharma, and K.M. George: *Mater. Sci. Eng. A*, 2014, vol. A589, pp. 174–81.
237. Y.G. Ko, C.S. Lee, and D.H. Shin: *Scripta Mater.*, 2008, vol. 58, pp. 1094–97.
238. A.V. Sergueeva V.V. Stolyarov, R.Z. Valiev, and A.K. Mukherjee: *Scripta Mater.*, 2000, vol. 43, pp. 819–24.
239. R.S. Mishra, V.V. Stolyarov, C. Echer, R.Z. Valiev, and A.K. Mukherjee: *Mater. Sci. Eng. A*, 2001, vol. A298, pp. 44–50.
240. A.V. Sergueeva V.V. Stolyarov, R.Z. Valiev, and A.K. Mukherjee: *Mater. Sci. Eng. A*, 2002, vol. A323, pp. 318–25.
241. J.H. Kim, S.L. Semiatin, and C.S. Lee: *Mater. Sci. Eng. A*, 2008, vol. A485, pp. 601–12.
242. S.V. Zherebtsov, G.A. Salishchev, R.M. Galeyev, O.R. Valiakhmetov, S.Yu. Mironov, and S.L. Semaitin: *Scripta Mater.*, 2004, vol. 51, pp. 1147–51.
243. P.E. Markovsky, O.M. Ivasishin, and V.V. Nemoshkalenko: in *Proc. Thermec 2000*, T. Chandra, K. Higashi, C. Suryanarayana, and C. Tome, eds., Elsevier Science Ltd., Amsterdam, The Netherlands, 2001.
244. S.L. Semiatin and J.J. Jonas: *Formability and Workability of Metals: Plastic Instability and Flow Localization*, American Society for Metals, Metals Park, OH, 1984.
245. O.M. Ivasishin and S.L. Semiatin: in *Proc. Thermec 2000*, T. Chandra, K. Higashi, C. Suryanarayana, and C. Tome, eds., Elsevier Science Ltd., Amsterdam, The Netherlands, 2001.
246. V.A. Gridnev, O.M. Ivasishin, and P.E. Markovskii: *Metal Sci. Heat Treatment*, 1985, vol. 25, pp. 43–48.
247. P.E. Markovsky: *Scripta Metall. Mater.*, 1991, vol. 25, pp. 2705–10.
248. O.M. Ivasishin, P.E. Markovsky, and E.I. Sharipov: *J. Mat. Prod. Techn.*, 1993, vol. 8, No. 2/3/4, pp. 204–12.
249. S.L. Semiatin and I.M. Sukonnik: in *Physical Simulation of Casting, Hot Rolling, and Welding*, H.G. Suzuki, ed., Dynamic Systems, Inc., Poestenkill, NY, 1997, pp. 395–405.
250. P.E. Markovsky and S.L. Semiatin: *Mater. Sci. Eng. A*, 2011, vol. A528, pp. 3079–89.
251. C.C. Chen: in *Process Modeling: Fundamentals and Applications to Metals*, T. Altan, H. Burte, H. Gegel and A. Male, eds, ASM, Metals Park, OH, 1980, pp. 365–86.
252. X. Ye, Z.T.H. Tse, G. Tang, Y. Geng, and G. Song: *Mater. Sci. Eng. A*, 2015, vol. A622, pp. 1–6.
253. S. Mironov, Y.S. Sato, and H. Hokawa: *J. Mater. Sci. Techn.*, 2018, vol. 34, pp. 58–72.
254. L. Zhou, H.J. Liu, P. Liu, and Q.W. Liu: *Scripta Mater.*, 2009, vol. 61, pp. 596–99.
255. A.L. Pilchak, W. Tang, H. Sahiner, A.P. Reynolds, and J.C. Williams: *Metall. Mater. Trans. A*, 2011, vol. 42A, pp. 745–62.

256. A.L. Pilchak and J.C. Williams: *Metall. Mater. Trans. A*, 2011, vol. 42A, pp. 773–94.
257. J. Su, J. Wang, R.S. Mishra, R. Xu, and J.A. Baumann: *Mater. Sci. Eng. A*, 2013, vol. A573, pp. 67–74.
258. S. Yoon, R. Ueji, and H. Fujii: *J. Mater. Proc. Technol.*, 2016, vol. 229, pp. 390–97.
259. D.G. Sanders, M. Ramulu, P.D. Edwards, and A. Cantrell: *J. Mater. Eng. Perf.*, 2010, vol. 19, pp. 503–09.
260. M.B. Uday, M.N. Ahmad Fauzi, H. Zuhailawati, and A.B. Ismail: *Sci. Techn. Welding Joining*, 2010, vol. 15, pp. 534–58.
261. A.R. McAndrew, P.A. Colegrove, C. Buhr, B.C.D. Flipo, and A. Vairis: *Prog. Mater. Sci.*, 2018, vol. 92, pp. 225–57.
262. M. Karadge, M. Preuss, C. Lovell, P.J. Withers, and S. Bray: *Mater. Sci. Eng. A*, 2007, vol. A459, pp. 182–91.
263. A.L. Pilchak and T.F. Broderick: *JOM*, 2013, vol. 65 (3), pp. 636–42.
264. A.E. Medvedev, A. Mendes, R. Lapovok, and S.L. Semiatin: *Mater. Sci. Eng. A*, 2018, vol. A737, pp. 253–64.
265. D. Hu, A. Dolganov, M. Ma, B. Bhattacharya, M.T. Bishop, and G.Z. Chen: *JOM*, 2018, vol. 70 (2), pp. 129–37.
266. A. Woodfield, E. Ott, J. Blank, M. Peretti, D. Linger, and L. Duke: *Mat. Sci. Forum*, 2009, vols. 618–619, pp. 135–38.
267. J.W. Foltz: in *Proc. 14th World Conference on Titanium*, 2019, in press.